

Article

An Archaeometric Analysis of Black-Appearing Iron Age Glass Beads from Vinha das Calças 4 (Portugal)

Valentina Lončarić ^{1,2,*} , Ana Margarida Arruda ³, Pedro Barrulas ^{1,2,4}  and Mafalda Costa ^{1,2,*} 

¹ HERCULES Laboratory, University of Évora, Palácio do Vimoso, Largo Marquês de Marialva 8, 7000-809 Évora, Portugal; pbarrulas@uevora.pt

² Associate Laboratory for Research and Innovation in Heritage, Arts, Sustainability and Territory IN2PAST, Évora University, Largo Marquês de Marialva 8, 7000-809 Évora, Portugal

³ UNIARQ—Centre for Archaeology of the University of Lisbon, School of Arts and Humanities, University of Lisbon, Alameda da Universidade, 1600-214 Lisbon, Portugal; ana2@campus.ul.pt

⁴ Department of Chemistry and Biochemistry, School of Sciences and Technology, University of Évora, 7004-516 Évora, Portugal

* Correspondence: vloncaric@uevora.pt (V.L.); mcosta@uevora.pt (M.C.)

Abstract: Phoenician colonisation of the Iberian Peninsula in the 1st millennium BCE introduced many novel and luxurious goods to the local populations of the Western Mediterranean. Among them, black-appearing glass beads are characteristic of indigenous female burials in Southern Portugal during the 6th century BCE. This study presents the results of the first comprehensive archaeometric investigation of black-appearing glass from Vinha das Calças 4 (Portugal), and of black-appearing glass from the Iberian Peninsula in general. A multi-analytical approach employing Stereomicroscopic observation of manufacture and use traces, VP-SEM-EDS, μ -XRD, and LA-ICP-MS was used to cover a wide range of questions regarding technology and provenance. All analysed samples are natron glass. All samples of black and white beads are characterized by high Zr and low Sr values typically ascribed to the use of Egyptian sands. A comparison of the results of previous studies from the same site clearly demonstrates at least two geochemical provenances for Phoenician-traded glass beads, located in the Levantine region and Egypt, respectively. Furthermore, different colours of glass in individual polychrome beads exhibit similar trace element patterns, which might suggest these beads could have been produced close to glassmaking sites/regions.

Keywords: Iron Age glass; black-appearing glass; Phoenicians; Iberian Peninsula; trace element analysis; VP-SEM-EDS; LA-ICP-MS; μ -XRD; Egypt



Citation: Lončarić, V.; Arruda, A.M.; Barrulas, P.; Costa, M. An Archaeometric Analysis of Black-Appearing Iron Age Glass Beads from Vinha das Calças 4 (Portugal). *Heritage* **2024**, *7*, 1265–1297. <https://doi.org/10.3390/heritage7030061>

Academic Editor: Artemios Oikonomou

Received: 16 January 2024

Revised: 14 February 2024

Accepted: 26 February 2024

Published: 29 February 2024



Copyright: © 2024 by the authors. Licensee MDPI, Basel, Switzerland. This article is an open access article distributed under the terms and conditions of the Creative Commons Attribution (CC BY) license (<https://creativecommons.org/licenses/by/4.0/>).

1. Introduction

The beginning of the 1st millennium BCE, roughly coinciding with the start of the Iron Age (IA) in the Mediterranean, saw a critical shift in glassmaking technologies from the Bronze Age tradition of using plant ash (HMG glass) and a mixed type of alkali (HMLK glass) to the increasing use of mineral soda, or natron, as a flux (LMG) [1–6]. Since natural occurrences of natron are geographically limited to evaporitic deposits in the Eastern Mediterranean [7], natron glass production would have to have been organised relatively close to natron sources to be cost-effective. Indeed, research into Iron Age glass compositions from the last few decades [1,2,8–11], including trace element and isotope studies [12–19], largely confirms the Eastern Mediterranean origin of mineral-soda-lime-silica glass ¹, with the two well-established regions during the whole 1st millennium BCE (and beyond) being Egypt and the Levantine coast. The produced glass was used to manufacture vessels and adornment objects (most notably beads and pendants) and traded across the Mediterranean and Continental Europe.

In Portugal, and the Iberian Peninsula in general, Iron Age glass beads are considered one of the many Eastern Mediterranean exotica traded by the Phoenicians ² during their

expansion and settlement in the West [12,32–37]. The reasons behind the Phoenician expansion in the West have long been debated—and at times contested—including exploitation of ores, territorial expansion, search for arable land, and resources like agricultural produce or cattle [27,28,38–40]. Isotopic study of silver hoards from Tell Dor, ‘Akko and ‘Ein Hofez (Israel) strongly suggests that the search for precious metals played a prominent role in the initial expeditions to the West [41]. In reality, all the above-stated motives likely played a part, if not in the initial Phoenician expeditions, then certainly in their later settlement in the West.

1.1. Historical Context

Archaeological evidence of Phoenician presence on the Iberian Peninsula dates from the 10th century BCE onwards, with early settlements in Huelva and (Gadir) Cádiz (Spain) during the 10th and 9th centuries BCE, and somewhat later, Portugal [32,33,42–44]. Phoenician expansion in modern-day Portugal relied on navigable routes along the coast and in the interior along the Guadiana, Sado, Tejo and Mondego rivers [33,42], as evidenced by littoral and estuarine sites like Castro Marim, Tavira, Setúbal, Lisbon, Quinta do Almaraz, and Alcáçova de Santarém, among others. The intensification of Eastern Mediterranean cultural inputs brought by the Phoenicians starting from 8th–7th c. BCE is referred to as “Orientalising”, characterised by the import of wine, red-slipped ware, textiles, Corinthian and Attic archaic pottery, alabaster vases, ostrich eggs and ivory, the introduction of urban planning, and the foundation of new settlements like Abul and Santa Olaia that assumed the role of commercial enclaves [33,45,46].

In the Portuguese interior, this process is somewhat delayed (late 7th/6th c. BCE onwards) and more selective compared to the coast, which is interpreted as the indigenous Iberian communities (re)negotiating their relationship with the Phoenician traders and settlers [34,47]. The difference between the coast and the interior is highlighted in the urban–rural dichotomy and consumption practices of Mediterranean goods. Whereas the littoral was becoming urbanised, the interior retained specific regional identities seen mainly in funerary practices and remained organised in small, open rural settlements [33,37,42]. In fact, early attempts to adopt Eastern Mediterranean architecture, evidenced by the construction in the late 9th c. BCE (radiocarbon dates) and later the destruction in the mid-8th c. BCE of the sanctuary on the acropolis of Castro dos Ratinhos (Moura, Portugal) [48], were quickly discarded and never revisited. Nevertheless, contact with the Phoenicians did not cease but instead focused on the procurement of luxury goods through, presumably, trade. Mediterranean goods in the interior are usually found in funerary contexts and mostly consist of adornments like beads, pendants, and amulets or other objects related to bodily care [34,37,46,49]. Of these, glass beads are easily the largest category, greatly surpassing their occurrence at coastal sites where they do not feature as part of funerary assemblages.

One of the notable examples of indigenous Iron Age sites in the Portuguese interior is Vinha das Calças 4, an enclosure necropolis located close to the modern-day city of Beja (Alentejo, Portugal). Archaeological research on the site took place in 2008 and 2009 to minimize the impact of the waterworks construction linked to the Alqueva water dam [1]. The necropolis includes over forty inhumation burials and several associated structures completely or partially enclosing some of the burials. The rectangular structures consist of ditches dug into bedrock to form an enclosure around burials 45 and 46, with two adjacent partially closed areas containing burials 38 and 48, as well as several burials dug within the negative structures themselves [50]. Closest parallels to this type of structures are found in the region at sites like Carlota, Cinco Reis and Palhais [42,51,52], forming the loosely defined regional group of enclosure necropolises in the Lower Alentejo (Portugal). The material assemblage discovered in the necropolis includes local forms of hand-built pottery, wheel-thrown red-fired and grey-fired pottery, bronze elements of attire and jewellery, bronze and iron belt buckles, iron spears and knives, gold and silver rings, pendants and beads, and a multitude of faience and glass beads [50]. In fact, vitreous artefacts are among the most notable finds from Vinha das Calças 4, with authors reporting

at least 1200 finds, consisting of 794 glass beads, 6 scarab or scaraboid amulets, and ca. 400 Egyptian faience discoid beads [50]. Like in other Iron Age funerary sites in Southern Portugal, black-appearing beads feature prominently at Vinha das Calças 4 [3,50]. However, black-appearing glass has not been the main focus of previous archaeometric studies of glass beads from the site [35,53]. This study therefore presents the first systematic scientific study of the phenomenon of black-appearing Iron Age glass from Portugal.

1.2. Black and Black-Appearing Glass

Black glass is a specific phenomenon since this colour is actually a result of an increased concentration of colourants which renders the glass of sufficient thickness black-appearing. The relationship between colourant concentration, glass thickness and transparency, as well as the lighting under which glass is observed can be summarized by Lambert–Beer Law:

$$I = I_0 \exp(-\epsilon cd);$$

where I = transmitted intensity at a considered wavelength, I_0 = the incident intensity at a considered wavelength, d = the thickness of the sample, c = the concentration of the colouring agent, and ϵ = the absorption coefficient [54]. In reality, hues of black-appearing glass are often reported as green, blue, purple, or brown when samples are observed under transmitted light or as thin layers [55–57], which can sometimes hinder the identification of black-appearing glass in the literature. However, even in the case of “black” glass, i.e., glass of non-perceivable hue, the colouring species are the same as those recorded for black-appearing/deeply coloured glass [55].

During the Late Bronze Age (LBA), dark or deeply coloured glass was produced by (usually) adding Mn, Co or Cu as a colourant [58,59]. A different colouring technology, not relying on high concentrations of any apparent element as a colourant is recorded somewhat later, from the 14th c. BCE [8,60,61]. Towards the end of LBA and in the early 1st millennium BCE the colouring technology of black glass appears to have switched to the preferential use of iron, as evidenced by finds from Pella (Jordan) [2], and early natron glass found in Italy [14,22], France, and Switzerland [1]. These early black natron glasses are considered a distinct compositional group due to their high iron and low lime contents and are interpreted as products of an experimental stage of natron glass production before the optimisation and later, standardisation of glassmaking recipes. Rather than being a separate ingredient, the high amount of iron was interpreted as the use of iron-rich sands which served as both the network former and the colouring agent [2,14,22]. Other notable types of black/deeply coloured Iron Age glass include a possibly small-scale Central European glass production using potash, as exemplified by black beads from Chotin (Slovakia) [14], and several locally produced natron glass beads from Sardis (Turkey) [21]. In all the mentioned cases, the colouring mechanism relies on varying amounts of iron. Alternative explanations of colouring technology to the standing theories of iron-rich sands acting both as a colourant and the vitrifier for Early Iron Age (EIA) black natron glass, including the use of hammer scale and iron welding, have recently been proposed for some darkly coloured iron-rich glasses from SE Europe [62].

During the Roman Imperial period, black-appearing glass was being produced on a large scale, with production technology changing through time and according to consumer demands. Four major groups of black Roman Imperial glass (1st–5th c. AD) defined on a large dataset from European and Mediterranean sites include (naturally) Fe-coloured plant-ash glass, Mn-coloured purple/black natron glass, Fe-coloured black natron glass, and an Fe-coloured black HIMT-like glass [56,57,63,64].

The phenomenon of black-appearing Iron Age glass in Portugal has so far mostly been covered from a typological and social perspective [3,34,37], with only a few samples subject to scientific analyses so far [35,53]. Current understanding of the Iron Age in Portugal distinguishes black glass beads as a geographically, chronologically, and contextually specific phenomenon [3,34,49], and may be summarised as follows:

Black-appearing glass in the IA context from Portugal occurs exclusively as beads, usually decorated with variations of eye motifs and their distribution is limited to the necropolises in Southern Portugal, namely the Algarve and Alentejo regions. A number of typological groups are documented, but the most common one includes beads decorated with “eye” motifs made by alternating layers of white and black, or sometimes, blue glass. The common decoration scheme for all groups of black-appearing glass is a high contrast between the darkly coloured body and the use of lightly coloured glass (usually white, and sometimes yellow) for the decoration patterns. Most assemblages can be dated to the 6th c. BCE, and their circulation does not seem to extend past the 5th c. BCE. Finally, unlike contemporary beads of other colours which appear in both funerary and non-funerary contexts, black-appearing beads are so far only known from funerary contexts, which could imply they held a specific symbolism in funerary dress.

2. Materials and Methods

2.1. Materials

The sample set comprised thirty-one “black” and white polychrome beads (Figure 1) from five female burials, randomly chosen among over one hundred and forty black-appearing beads. Burials 13, 40, 47, 48 were anthropologically sexed as female, while burial 27 was identified as archaeologically female on the basis of grave goods and funerary attire, which is in conformation with the current understanding of Iron Age funerary practices in the Portuguese interior [34,46,50,65]. Because of their delicate state, sample preparation procedures were omitted for the majority of the samples. Fragments of three samples from (VC-24, VC-110, VC-129) were mounted in resin and hand polished on a silicon carbide paper to remove altered glass layers and cleaned with distilled water in an ultrasonic bath for 5 min to dislodge any contaminating particles. The polished samples served as a control for the potential effects of leaching and/or glass corrosion on the results of the non-polished samples.

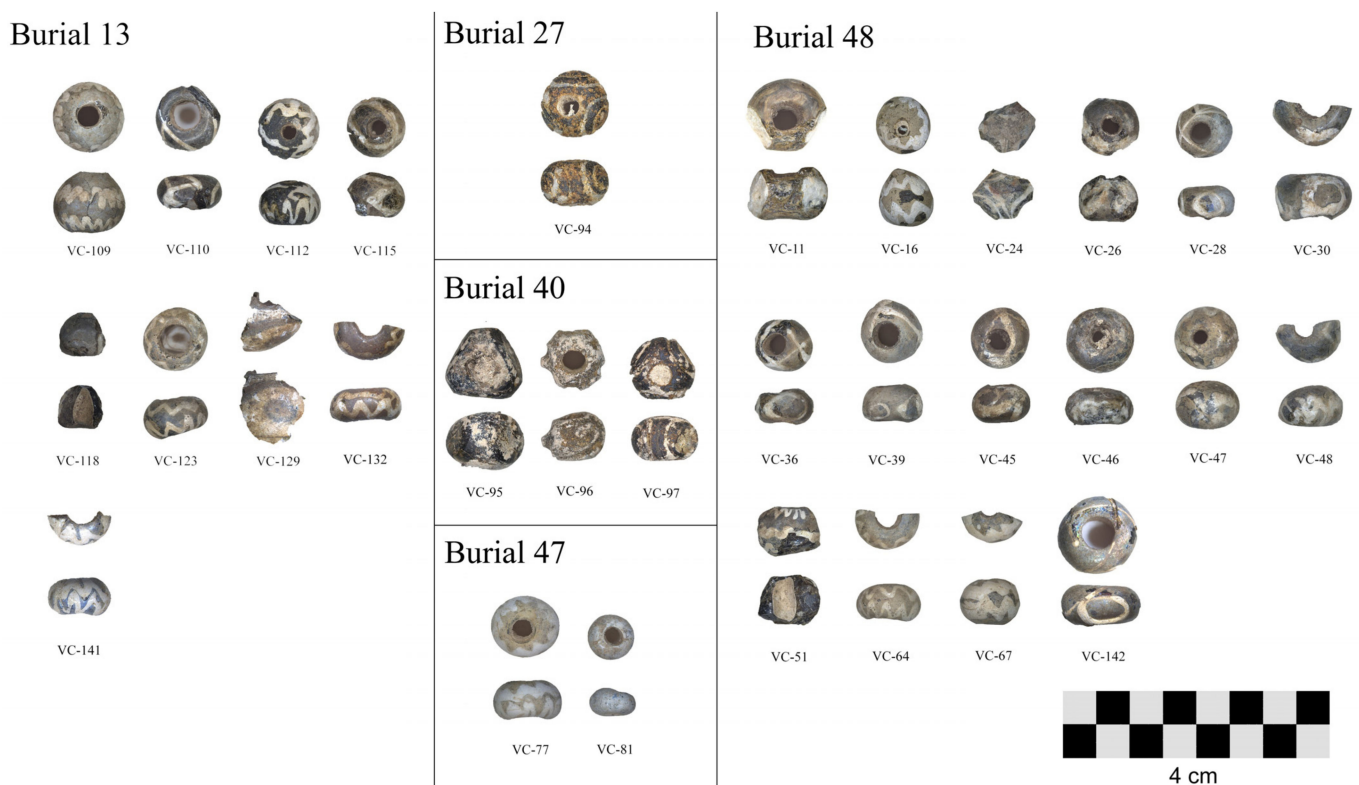


Figure 1. Black-appearing glass beads from Vinha das Calças 4 analysed in this study.

2.2. Methods

Analytical techniques were chosen in accordance with previously published studies of glass beads and other vitreous material from Vinha das Calças 4 [35,53,66,67] to allow comparison with published results. The procedure included stereomicroscopical examination, micro-X-Ray diffraction (μ -XRD), variable pressure scanning electron microscopy with energy dispersive spectrometry (VP-SEM-EDS), and laser-ablation inductively coupled plasma-mass spectroscopy (LA-ICP-MS).

2.2.1. Optical Microscopy

Optical examination of the beads served to document the samples prior to analysis, assess the state of preservation, and identify characteristic signs of degradation and bead manufacture traces. All the samples were initially examined by a Leica M205C stereomicroscope (Leica Microsystems, Mannheim, Germany) mounted with a Leica MC170 HD camera (Leica Microsystems, Mannheim, Germany) for image acquisition. Samples were observed at different magnifications, ranging from 7.8 \times to 160 \times .

2.2.2. μ -XRD

All the samples were analysed with a BrukerTM D8 Discover[®] diffractometer (Bruker AXS GmbH, Karlsruhe, Germany), using a Cu K α radiation source (40 kV, 40 mA), a Göebel mirror, a 1-mm collimator, and a LYNXEYE linear detector. Analysis conditions included a 2 θ angular range of 3–75 $^\circ$, with a step size of 0.05 $^\circ$ and a step time of 1 s. All analyses were carried out in micro configuration on black and white glass portions where observable. Crystalline phases were identified in DIFFRAC.SUITE.EVA[®] software (version 5.1) by search-matching the acquired patterns with those available in the Powder Diffraction File (PDF-2) X-ray patterns database of the International Centre for Diffraction Data.

2.2.3. VP-SEM-EDS

All samples were imaged in backscatter (BSE) mode with a HitachiTM S3700N scanning electron microscope (Hitachi High-Technologies Corporation, Tokyo, Japan) in variable pressure (VP) mode. Elemental mapping and spectral data acquisition were performed using a QUANTAX EDS microanalysis system with a BrukerTM XFlash 630M EDS Detector[®] (Bruker Nano GmbH, Berlin, Germany). Analysis conditions for all samples included low vacuum (40 Pa), 20 kV accelerating voltage and a working distance of 9–13 mm. Spectral data were processed in BrukerTM ESPRIT compact software package (version 2.3.1.1019) using standardless quantification and the obtained compositions were calculated as normalised oxide wt. %.

2.2.4. LA-ICP-MS

All samples were analysed with an AgilentTM 8800 Triple Quad ICP-MS (Agilent Technologies Inc., Palo Alto, CA, USA) and a CETAC LSX-213 G2 + (Teledyne Technologies, Omaha, NE, USA) laser ablation system for micro-sampling and sample introduction. Laser ablation system conditions for the thirty-one samples are provided in Table 1. ICP-MS analysis conditions are given in Table 2. Analysis conditions, ICP-MS calibration, performance monitoring and post-processing followed earlier studies of vitreous material from Vinha das Calças 4 [35,67]. System calibration was performed using the SRM NIST 610. The initial signal corresponding to surface layers was discarded to minimise the effect of glass alteration. Data processing was performed in the GLITTER[®] software (version 4.5), using the SRM NIST 610 as a primary reference material, and SiO₂ concentrations detected by VP-SEM-EDS as the internal standard in archaeological samples. SRM NIST 610 was periodically analysed during each run. SRM NIST 612 was analysed following SRM NIST 610, and periodically after three to five archaeological samples (depending on whether one or two colours of glass were analysed for the archaeological sample) during each run as a quality control sample, for a total of 36 measurements. SRM NIST 610 and SRM NIST 612 results, including average concentrations, standard deviations, accuracy (RD%),

and precision (RSD%) are reported in Table S1 (Supplementary Information). Minimum detection limits (DL) calculated in the GLITTER[®] software for the analysed SRM varied between 62 and 0.01 ppm for major elements, and 0.001 and 3.42 ppm for trace elements. The full list of associated DL estimates for SRM NIST 610 and SRM NIST 612 are available in Table S1.

Table 1. Laser ablation system (CETAC LSX-213 G2 +) conditions.

Laser energy output	100%
Analysis mode	spot
Spot size	50 µm
Repetition rate	20 Hz
Burst count	600
Carrier gas (He) flow	0.8 L/min
Run	55 s
Gas blank	15 s
Ablation	30 s
Washout	10 s

Table 2. Agilent[™] 8800 Triple Quad ICP-MS conditions, including analysed elements and their respective dwell times.

Acquisition mode	time-resolved analysis (TRA)
Scan type	MS/MS
Plasma parameters	
RF power	1200
RF matching	1.25 V
Sample depth	4.0 mm
Carrier gas (He)	0.6 L/min
Plasma gas (Ar)	15 L/min
Analysis mode	no gas
Dwell times	
2 ms	²³ Na; ²⁸ Si; ⁵⁶ Fe; ⁵⁷ Fe
5 ms	²⁴ Mg; ²⁷ Al; ³⁹ K; ⁴³ Ca; ⁴⁴ Ca; ⁵⁵ Mn
10 ms	⁴⁷ Ti; ⁵¹ V; ⁵² Cr; ⁵⁹ Co; ⁶⁰ Ni; ⁶³ Cu; ⁶⁶ Zn; ⁸⁵ Rb; ⁸⁸ Sr; ¹³⁷ Ba; ²⁰⁸ Pb
20 ms	⁷⁵ As; ⁸⁹ Y; ⁹⁰ Zr; ⁹³ Nb; ¹¹⁸ Sn; ¹²¹ Sb; ¹³⁹ La; ¹⁴⁰ Ce; ¹⁴¹ Pr; ¹⁴⁶ Nd; ¹⁴⁷ Sm; ¹⁵³ Eu; ¹⁵⁷ Gd; ¹⁵⁹ Tb; ¹⁶³ Dy; ¹⁶⁵ Ho; ¹⁶⁶ Er; ¹⁶⁹ Tm; ¹⁷² Yb; ¹⁷⁵ Lu; ¹⁷⁸ Hf; ¹⁸¹ Ta; ²⁰⁹ Bi; ²³² Th; ²³⁸ U

Three to four spots were analysed on each archaeological sample, depending on surface morphology, and the results averaged for each sample. Although white glass decorations were analysed wherever they visually appeared reasonably preserved, analyses of samples VC-24w, VC30w, VC-36w, VC-39w, VC-45w, VC-47w, VC-64w, VC-67w, VC-112w, VC-115w, VC-132w, VC142w are considered non-reproducible because of extensive alteration and high heterogeneity (RSD > 33%) for repeated measurements and are therefore excluded from consideration. For all other obtained results presented in Section 3 and Results and Discussion, Cl, S, and P measured by EDS were added, and the total composition of all elements was normalised to 100.

3. Results and Discussion

3.1. Typology and Bead Manufacture

3.1.1. Typology

Three distinct types of beads, according to the decoration, were identified among the studied set, as well as several examples (VC-11, VC-81, VC-118) which do not fit in the general typology observed on the site, or for black-appearing beads in general [3]. In the remainder of the text, these samples are referred to as “other beads”.

The first and most numerous ³ type is represented by thirteen (VC-16, VC-46, VC47, VC-48, VC-51, VC-64, VC-67, VC-77, VC-109, VC-112, VC-123, VC-132) small beads ($d < 14$ mm) with one or more wavy lines along the circumference of the bead. This type of beads is actually considered a rare occurrence among black-appearing beads in Portugal [3], and their abundance at Vinha das Calças 4 is an interesting exception.

Typical “eye” beads are less represented in the necropolis assemblage ⁴, in stark contrast to other sites with black-appearing beads [3]. They are represented by six beads (VC-24, VC-30, VC-94, VC-95, VC97, VC-129), both as large ($d > 14$ mm) and small ($d < 14$ mm) beads ⁵. Furthermore, fragments of the large “eye” bead VC-24 clearly show that the bead originally had the eye decoration organised in two rows along the bead circumference, which is a variation observed in other black-appearing bead assemblages from Portugal [3]. Following a recently proposed typological classification for Iron Age “eye” beads in Southern Portugal [49], these beads belong to F. Gomes’ Group 1: Annular beads, Sub-Variant 1.b.1.b: “‘Black’ matrix with white and ‘black’ eyes”, and Group 2: Spherical Beads, Sub-Variant 2.c.1.b: “‘Black’ matrix with white and ‘black’ eyes”. In this study, “eye” beads are not split into further types since the basic motif, and to an extent, the manufacturing technique (see below), remain the same.

The third type is represented by nine (VC-26, VC-28, VC-36, VC-39, VC-45, VC-96, VC-110, VC-115, VC142) small ($d < 14$ mm) beads with a spiral or “pseudo-eye” ornamentation made by looping or trailing a single strand of glass paste around the perforation to create three interconnected eye motifs. This type of bead constitutes a significant number of black-appearing beads from the site ⁶. This type is not specifically reported for other Portuguese sites [3], nor does it match the descriptions for other published black Iron Age glass [14,22]. Other occurrences of this type of glass beads explicitly mentioned either for Portugal or other regions have not been found in the literature.

Finally, samples VC-11 and VC-81 do not present features typical of black-appearing beads. The remains of white glass on bead VC-11 suggest two circular decorations, possibly “eyes” were added to the body. Due to the brown-and-black streaked appearance of the body, the bead was classified as black-appearing. Sample VC-81 has no discernible decorations, and is tentatively classified as a black-appearing bead because of the similarity of the light alteration layer to those observed on other black-appearing beads.

3.1.2. Bead Manufacture

Optical microscopy of the beads revealed traces characteristic of wire-winding, including spherical bubbles in sections of fragmented beads (Figure 2 centre), asymmetric profiles (e.g., VC-48 in Figure 1), and glass trails around perforation edges (Figure 2, left). Bubbles in glass result from gasses being trapped in the solidifying melt and their shape can be indicative of the way glass was stretched during the working stage. Spherical bubbles in bead cross-section, therefore, evidence that the gather was wound around the mandrel, as opposed to elongated bubbles observable in drawn beads, or glass vessels [68,69]. A large discontinuity in the perforation wall, arising from an incomplete attachment of the viscous glass coils during winding [70], was also observed in sample VC-110 (Figure 2, right). Glass trails, another feature highly indicative of bead winding [70,71], were noted in several examples (Figure 2, left, right). The white decorations on the beads were applied on the viscous bead core, either by one or more continuous motions in the case of beads with waved line decorations and beads with a triple spiral motif (Figure 2, right), or by

superimposing layers of white and black glass in the case of eye beads (VC-24, VC-94, VC95, VC-97, VC-129), with the exception of uneven white decoration on sample VC-30 which appears to have been made by directly drawing the eye motif with white glass in the bead body instead of layering different colours. In some cases (VC-95, VC-97), layers of white glass in the eye beads were not preserved, leading to the detachment of the superimposed layers of the eye decoration and lending the beads a triangular prismatic appearance. Based on the observed traces, all the analysed black-appearing beads can be classified as wire-wound beads, made by winding viscous glass around a mandrel, similar to modern-day lampworking, which is a well-documented technique on prehistoric glass beads [62,71–74].

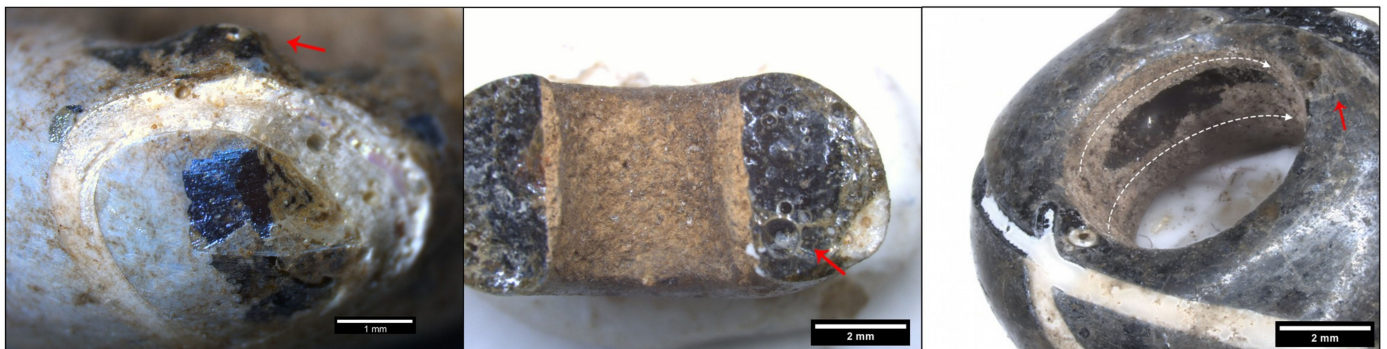


Figure 2. Glass alteration and manufacture traces documented on the samples from Vinha das Calças 4. **Left:** VC-28, detail of the bead showing the difference between the light blue leached layer and the exposed black-appearing glass. The white decoration exhibits a porous and irregular appearance consistent with a higher degree of degradation. The red arrow points to a glass trail on the perforation edge; **Centre:** VC-132, cross-section with remains of the bead release. The red arrow points to a large round bubble indicative of bead winding; **Right:** VC-110, detail of the perforation with a large discontinuity. White dashed arrows highlight a possible direction of glass winding. The red arrow points to a glass trail on the perforation edge.

3.2. State of Preservation

Macro- and microscopic evidence of degradation such as surface porosity, surface damage, fracturing, iridescence, and the formation of discoloured dealcalinised layers (Figure 3, left), was observed to some extent in all the studied beads. White glass decorations appear to be more susceptible to degradation than black glass and are completely absent in some beads (VC-95, VC-96). A surface layer of altered glass resulting from alkali leaching [75–77] was noted in practically all samples. The colour of this layer is highly variable among the beads and covers a range of colours ranging from white to blue-grey, hindering accurate description of the true hue of black-appearing glass. Altered layers are extremely brittle and detached easily during handling, which, in conjunction with the characteristic typology of the samples, allowed for their identification as black, or black-appearing beads since in many cases it exposed the underlying glass bulk. VP-SEM-EDS observations of the beads further highlighted the extent of degradation (Figure 3). The surface of the beads is covered by a silica-rich, dealcalinised layer covering both the black-appearing and white glasses, which occasionally made the identification of glass colours by VP-SEM-EDS challenging because of the lack of contrast. In the areas where this surface layer is detached, different colours of glass were easily identified due to the high BSE contrast arising from the presence of opacifier crystals in the white glass. These exposed areas are marked by an irregular texture with a reticulate network of ridges, cracks, especially on the borders of different glass colours, and collapsed bubbles, often filled with organic detritus (Figure 3, right).

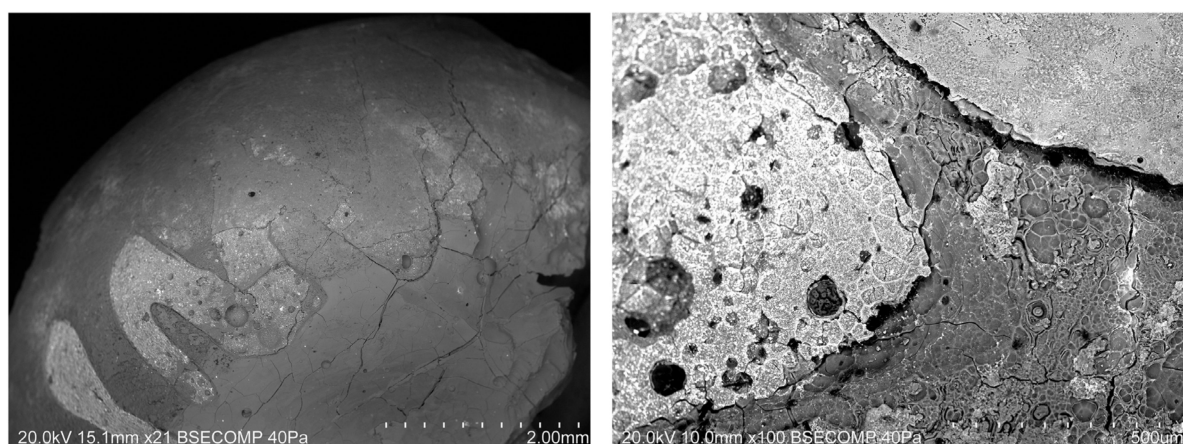


Figure 3. VP-SEM-EDS image of samples VC-51 (left) and VC-109 (right) showing the difference in opacifier crystals (seen as bright areas in BSE images) observable in the altered, silica-rich layers of white glass decorations and the exposed white glass bulk.

Overall low Na_2O values detected by EDS in non-polished samples (<0.1–16.2 wt. %, avg. 1.7, Table S2—Supplementary Information), coupled with a relative enrichment in silica (15.2–86.2 wt. %, avg. 73.4) are clearly indicative of extensive degradation. Such an extent of alteration was not observed on previously studied blue, turquoise, white, colourless and yellow glass from the site [35], suggesting the apparent chemical instability of black-appearing beads might arise from a significant compositional difference compared to previously analysed beads from Vinha das Calças 4. A possible relationship between the chemical composition and colour of the studied beads and their susceptibility to aqueous attack is further discussed in Section 3.3. Considering the surface-sensitive nature of EDS analysis and the impossibility of mounting and polishing all of the samples, LA-ICP-MS proved to be a crucial technique for accurate study of major and minor (Table 3), as well as the trace element composition due to the possibility of sampling the pristine glass by laser ablation. Even so, eight samples of white glass (VC-16w, VC-26w, VC-28w, VC-77w, VC-109w, VC-110w, VC-123w, VC-141w,) were found to be extremely leached ($\text{Na}_2\text{O} + \text{K}_2\text{O} < 1.5$ wt. %) and should be considered with caution when mentioned in further discussion.

Table 3. Major and minor oxide concentrations for the studied beads. All oxides expressed as wt. %. LA-ICP-MS data unless indicated otherwise (*).

Sample	Colour	Na_2O	MgO	Al_2O_3	SiO_2 *	P_2O_5 *	SO_3 *	Cl *	K_2O	CaO	TiO_2	MnO	FeO	CoO	CuO	SnO_2	Sb_2O_3	PbO
VC-11bl	"black"	16.6	0.4	0.4	71.2	<0.1	0.6	<0.1	0.2	7.2	0.1	<0.1	3.3	<0.1	<0.1	<0.1	<0.1	<0.1
VC-11w	white	16.3	0.3	0.4	69.6	<0.1	<0.1	0.8	0.1	6.1	<0.1	<0.1	0.2	<0.1	<0.1	<0.1	<0.1	6.0
VC-112bl	"black"	16.5	0.4	0.5	68.3	<0.1	0.3	1.1	0.6	7.6	<0.1	<0.1	4.5	<0.1	<0.1	<0.1	<0.1	<0.1
VC-16bl	"black"	16.2	0.4	0.5	69.2	0.1	0.4	0.9	0.5	7.4	<0.1	<0.1	4.3	<0.1	<0.1	<0.1	<0.1	<0.1
VC-16w	white	0.2	0.3	0.9	90.4	0.4	0.2	0.3	<0.1	1.9	0.2	<0.1	1.1	<0.1	<0.1	<0.1	4.1	<0.1
VC-24bl	"black"	15.6	0.4	0.5	68.7	0.4	0.2	0.9	0.3	7.6	<0.1	<0.1	5.0	<0.1	<0.1	<0.1	0.3	<0.1
VC-26bl	"black"	17.1	0.5	0.8	68.8	<0.1	1.5	0.3	0.4	7.7	0.1	<0.1	2.8	<0.1	<0.1	<0.1	<0.1	<0.1
VC-26w	white	<0.1	0.4	0.3	88.8	<0.1	0.3	1.0	<0.1	8.3	0.2	<0.1	0.5	<0.1	<0.1	<0.1	<0.1	<0.1
VC-28bl	"black"	17.3	0.5	1.0	68.1	<0.1	<0.1	0.7	0.6	8.9	<0.1	<0.1	2.6	<0.1	<0.1	<0.1	<0.1	<0.1
VC-28w	white	<0.1	0.4	0.5	89.2	<0.1	0.2	0.3	<0.1	6.2	0.1	<0.1	0.3	<0.1	<0.1	<0.1	2.6	<0.1
VC-30bl	"black"	16.6	0.4	0.6	68.5	0.3	0.7	<0.1	0.2	6.5	0.1	<0.1	5.8	<0.1	<0.1	<0.1	<0.1	<0.1
VC-36bl	"black"	17.8	0.5	1.0	66.8	0.2	0.3	0.7	0.5	7.5	0.1	<0.1	4.5	<0.1	<0.1	<0.1	<0.1	<0.1
VC-39bl	"black"	17.1	0.5	1.0	68.8	<0.1	0.1	0.2	0.6	7.6	0.1	<0.1	3.8	<0.1	<0.1	<0.1	<0.1	<0.1
VC-45bl	"black"	16.9	0.4	1.2	67.9	0.4	0.9	0.2	0.8	6.9	0.1	<0.1	4.1	<0.1	<0.1	<0.1	<0.1	<0.1
VC-46bl	"black"	16.3	0.5	0.5	68.9	<0.1	0.3	0.4	0.6	7.5	<0.1	<0.1	4.7	<0.1	<0.1	<0.1	<0.1	<0.1
VC-46w	white	16.8	0.5	0.4	68.4	<0.1	<0.1	1.2	0.5	7.8	<0.1	<0.1	0.2	<0.1	<0.1	<0.1	4.1	<0.1
VC-47bl	"black"	17.0	0.4	0.5	69.2	<0.1	0.2	0.3	0.5	7.5	<0.1	<0.1	4.1	<0.1	<0.1	<0.1	<0.1	<0.1
VC-48bl	"black"	17.1	0.5	0.5	69.1	<0.1	<0.1	0.5	0.8	7.5	<0.1	<0.1	3.9	<0.1	<0.1	<0.1	<0.1	<0.1
VC-48w	white	14.5	0.5	0.7	71.9	<0.1	<0.1	0.7	0.4	6.3	0.1	<0.1	0.4	<0.1	0.2	<0.1	4.4	<0.1
VC-51bl	"black"	17.7	0.4	0.6	69.1	<0.1	0.6	0.5	0.5	6.8	0.1	<0.1	2.3	<0.1	<0.1	<0.1	0.6	0.3
VC-51w	white	14.6	0.4	0.7	70.7	<0.1	0.6	0.6	0.3	7.2	0.2	<0.1	2.6	<0.1	<0.1	<0.1	1.4	0.2
VC-64bl	"black"	16.5	0.6	0.8	66.2	0.2	0.1	0.1	0.6	8.2	0.1	<0.1	6.3	<0.1	<0.1	<0.1	<0.1	<0.1
VC-67bl	"black"	16.9	0.4	0.4	69.8	0.2	0.8	0.5	0.4	7.5	<0.1	<0.1	3.0	<0.1	<0.1	<0.1	<0.1	<0.1
VC-95bl	"black"	17.1	0.4	0.5	69.1	<0.1	<0.1	1.1	0.2	6.0	0.1	<0.1	5.4	<0.1	<0.1	<0.1	0.2	<0.1

Table 3. Cont.

Sample	Colour	Na ₂ O	MgO	Al ₂ O ₃	SiO ₂ *	P ₂ O ₅ *	SO ₃ *	Cl *	K ₂ O	CaO	TiO ₂	MnO	FeO	CoO	CuO	SnO ₂	Sb ₂ O ₃	PbO
VC-97bl	"black"	14.3	0.5	0.6	66.2	<0.1	<0.1	0.4	0.2	9.1	<0.1	<0.1	7.6	<0.1	<0.1	<0.1	1.0	<0.1
VC-77bl	"black"	16.0	0.5	0.6	70.0	<0.1	<0.1	<0.1	0.6	7.9	<0.1	<0.1	4.2	<0.1	<0.1	<0.1	<0.1	<0.1
VC-77w	white	0.1	0.4	0.7	90.8	<0.1	<0.1	0.2	<0.1	4.4	<0.1	<0.1	0.4	<0.1	<0.1	<0.1	2.9	<0.1
VC-81b	blue	16.9	0.4	0.6	71.1	<0.1	0.7	0.2	0.6	8.0	0.1	<0.1	0.5	<0.1	0.7	<0.1	<0.1	<0.1
VC-94bl	"black"	14.6	0.5	0.5	66.9	<0.1	<0.1	1.4	0.2	10.0	<0.1	<0.1	5.4	<0.1	<0.1	<0.1	0.4	<0.1
VC-96bl	"black"	15.1	0.6	0.8	71.8	<0.1	0.3	0.9	0.4	6.9	0.2	<0.1	2.2	<0.1	<0.1	<0.1	0.2	0.5
VC-109bl	"black"	17.0	0.4	0.7	68.0	0.2	0.7	0.4	0.5	7.3	0.1	<0.1	2.6	<0.1	<0.1	<0.1	1.2	0.2
VC-109w	white	0.2	0.4	0.7	88.1	0.2	0.7	0.4	<0.1	4.6	<0.1	<0.1	0.6	<0.1	<0.1	<0.1	4.0	<0.1
VC-110bl	"black"	16.4	0.4	0.8	70.2	<0.1	1.9	<0.1	0.4	7.1	<0.1	<0.1	2.7	<0.1	<0.1	<0.1	<0.1	<0.1
VC-110w	white	0.2	0.3	0.8	87.3	<0.1	2.1	<0.1	<0.1	3.4	<0.1	<0.1	0.8	<0.1	0.2	<0.1	4.6	<0.1
VC-115bl	"black"	16.8	0.4	0.7	68.5	<0.1	0.5	0.5	0.4	7.9	<0.1	<0.1	2.8	<0.1	<0.1	<0.1	<0.1	0.3
VC-118	"black"	16.5	0.4	0.7	69.8	<0.1	0.4	0.7	0.4	7.1	0.1	<0.1	3.7	<0.1	<0.1	<0.1	<0.1	<0.1
VC-123bl	"black"	16.1	0.5	0.5	69.5	<0.1	0.2	0.4	0.8	7.8	<0.1	<0.1	4.1	<0.1	<0.1	<0.1	<0.1	<0.1
VC-123w	white	0.3	0.4	1.1	83.8	<0.1	0.1	0.3	<0.1	5.7	<0.1	<0.1	0.9	<0.1	0.1	<0.1	7.1	<0.1
VC-129bl	"black"	15.9	0.4	0.4	69.8	<0.1	0.1	1.2	0.2	7.0	<0.1	<0.1	4.6	<0.1	<0.1	<0.1	<0.1	<0.1
VC-129w	white	14.5	0.3	0.4	65.4	0.1	0.3	1.3	0.1	6.6	<0.1	<0.1	0.2	<0.1	<0.1	<0.1	10.6	<0.1
VC-132bl	"black"	16.8	0.4	0.5	68.6	<0.1	<0.1	0.9	0.7	7.7	<0.1	<0.1	4.3	<0.1	<0.1	<0.1	<0.1	<0.1
VC-141bl	"black"	16.4	0.4	0.5	69.6	<0.1	0.2	1.1	0.6	7.6	<0.1	<0.1	3.5	<0.1	<0.1	<0.1	<0.1	<0.1
VC-141w	white	0.1	0.4	0.6	89.6	<0.1	<0.1	0.1	<0.1	4.6	0.1	<0.1	0.6	<0.1	0.2	<0.1	3.6	<0.1
VC-142bl	"black"	17.7	0.5	1.1	67.4	<0.1	0.8	<0.1	0.6	8.9	<0.1	<0.1	2.8	<0.1	<0.1	<0.1	<0.1	<0.1

* Analysed by VP-SEM-EDS.

3.3. Glassmaking Technology

3.3.1. Fluxing Agent

Major glassmaking technologies are defined on the basis of the fluxing agent used, namely a mineral soda source (generally agreed to have been natron) which does not contribute to the MgO and K₂O content of the glass, halophytic plant ash which results in high MgO content, wood-ash glass which results in high K₂O and MgO, and low Na₂O, and the use of "mixed alkali" flux typical of European LBA glassmaking technology resulting in (relatively) high K₂O and low MgO [78]. Although MgO and K₂O values detected on bead surface by VP-SEM-EDS range from <0.1 wt. % to 3.5 wt. % and from <0.1 wt. % to 1.5 wt. % for MgO and K₂O, respectively (Table S2), low concentrations of these oxides (<0.6 wt. % MgO, <0.9 wt. % K₂O) in the glass bulk detected by LA-ICP-MS suggest all samples could be classified as natron glass or mineral-soda lime glass if the effects of leaching and surface contamination are considered. Oxide concentrations detected by VP-SEM-EDS in polished samples VC-24, VC-110, and VC-129 (Table S2—Supplementary Information) confirm this conclusion as their alkali values, aside from sample VC-24w, fall well within the natron glass range. When measurements of the glass bulk by LA-ICP-MS are considered, the effect of leaching tends to be less pronounced in black-appearing glass (14.3–17.8 wt. % Na₂O) compared to white glass decorations (<0.1–16.9 wt. % Na₂O) which tend to have low alkali contents even when sampled by laser ablation (Table 3). A ternary diagram of Na₂O–MgO + K₂O–CaO [78], as well as a typically high alkali ratio (<0.95) [79], illustrate that all relatively preserved (Na₂O + MgO + K₂O > 10 wt. %) samples can be characterized as mineral soda-lime-silica glass, or natron glass (Figure 4), which is in accordance with the current understanding of Iron Age glass exchange in the Western Mediterranean [12,35,36,53,80].

3.3.2. Network Former

The main source of silica (SiO₂) used as the network former in soda-lime-silica glass is quartz, added either in the form of (crushed) pebbles or as sufficiently pure quartz-rich sand. To a lesser extent, both Ti and Al may substitute for Si in the crystalline structure of quartz, but their content in glass is usually taken as an indicator of mineral impurities such as feldspars, clays, pyroxene, rutile and Fe-Ti oxides [81]. Alumina in particular is indicative of silica purity since it is highly abundant in sand deposits as the clay fraction. All the analysed samples from Vinha das Calças 4 exhibit low Al₂O₃ values (0.33–1.2 wt. %) as well as low TiO₂ (0.06–0.21 wt. %). Low amounts of these oxides related to mineral impurities in sand suggest the use of a highly pure silica source.

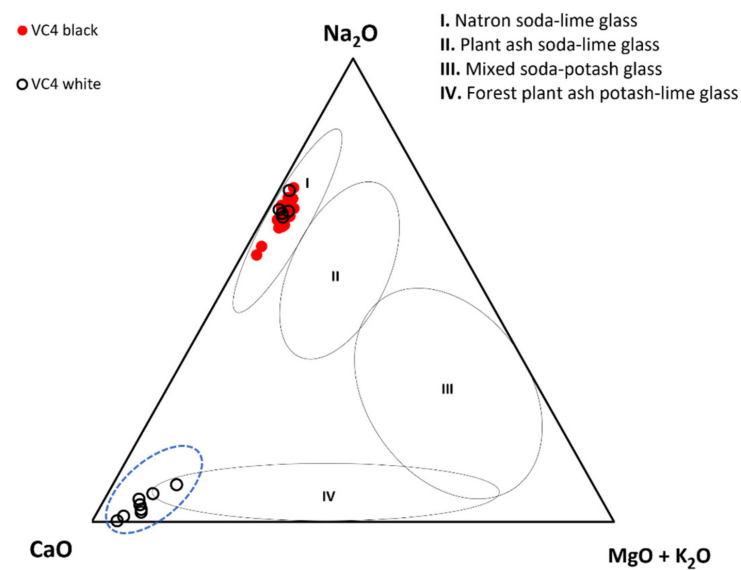


Figure 4. Na₂O–MgO + K₂O–CaO ternary diagram of the analysed black-appearing beads from Vinha das Calças 4 (LA-ICP-MS data). Extremely leached samples (VC-16w, VC-26w, VC-28w, VC-77w, VC-109w, VC-110w, VC-123w, VC-141w,) are highlighted by the dashed ellipse. Glass family ranges from [78].

Until recently, low-Al (<1.5 t.%) natron glass has mostly been reported sporadically [1,9,22,25,82,83]. Notable datasets which identify low-Al glass as a characteristic compositional group include some Hellenistic vessels from the 3rd c. BCE votive deposit at Satricum (group “Satricum A”) [20], 2nd c. BCE Mediterranean III vessels from Italy [13], data on Iron Age glass beads from Slovenia, Croatia, and Bosnia and Herzegovina [62], and some translucent Hallstatt period glass beads from Poland [25]. Other notable sets in the Mediterranean include Early Iron Age (EIA) natron glass from South Italy [22], Iron Age glass from Mallorca (Spain) [12], and black-appearing glass from Carthage (Tunisia) [80]. Although later in date, the Egyptian 1 (Eg 1) group of Celtic glass also displays similar alumina content [17]. The similarity of the silica source used for the production of black-appearing glass beads from Vinha das Calças 4 to other 1st millennium BCE low-Al glass is illustrated in Figure 5. Titania and alumina ratios of the studied beads show a good overlap with low-Al natron glass from SE Europe [62], black glass from Carthage (Tunisia) [80], and S Italy [22,84]. Drastically higher titania–silica and lower alumina–silica ratios for low-Al glass indicate that this type was made with a silica source different from the alumina-rich sand used for the production of high-Al Mediterranean Group II core-formed glass vessels from Satricum (Satricum B and C) (Italy) [20] and Mediterranean Group I and II vessels from Adria (Italy) [13], as well as Iron Age glass beads of Levantine origin from Vinha das Calças 4 (Portugal) [35] and Mallorca (Spain) [12] (Figure 5A). The studied samples also differ in titania–silica–alumina ratios from EIA black glass from Italy [14,22,84], which groups closer to low-Al natron glass from Son Mas (Mallorca, Spain), low-Al Mediterranean Group II glass vessels from Satricum (Italy) [20], and Mediterranean Group III vessels from Adria (Italy) [13]. Although visually similar to the high-Fe EIA black glass representative of early natron glass production [1,2,14,22], black-appearing beads from Vinha das Calças 4 are characterised both by the use of a purer silica source, and lower amounts of iron, comparable to the black glass from Carthage [80] (Figure 5B).

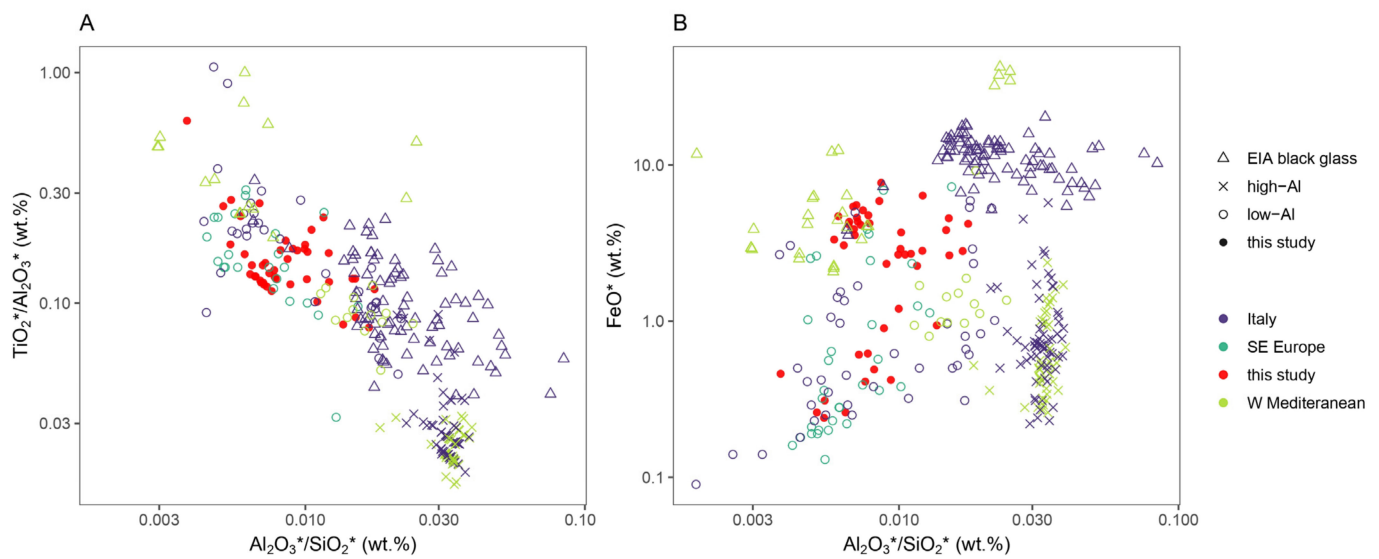


Figure 5. (A) $\text{TiO}_2^*/\text{Al}_2\text{O}_3^*$ – $\text{Al}_2\text{O}_3^*/\text{SiO}_2^*$ biplot showing the differences and similarities in silica sources used to produce black-appearing beads from Vinha das Calças 4 (this study, LA-ICP-MS data) and comparative Iron Age glass from various assemblages. (B) FeO^* – $\text{Al}_2\text{O}_3^*/\text{SiO}_2^*$ biplot demonstrating the addition of iron colourant to black-appearing beads from Vinha das Calças 4 (this study) compared to other Iron Age glass from various assemblages. All values normalized (*) to the sum of 8 oxides (Na_2O , MgO , Al_2O_3 , SiO_2 , K_2O , CaO , TiO_2 , FeO). Explanation of comparative dataset: Italy—natron and black glass beads from Sarno, Cumae, and Capua [22], black glass beads from Bologna, Pozzuoli and Cumae [14], natron and black glass beads from Francavilla Marittima, Torre Galli and Amendolara [84], Mediterranean Group I, II, III vessels from Adria [13], Mediterranean Group II vessels from Satricum [20]; SE Europe—low-Al natron glass beads from Una River Valley and Sanski Most (Bosnia and Herzegovina), Turska Kosa, Istria, Kompolje, Smiljan, Ljubač and Pannonia (Croatia) [62]; W Mediterranean—black glass beads from Carthage (Tunisia) [80], Levantine natron glass beads from Vinha das Calças 4 [35], natron glass from Son Mas (Mallorca, Spain) [12]; EIA black glass—soda-lime-silica samples reported as black glass [14,22,80]; high-Al— $\text{Al}_2\text{O}_3 > 1.5$ wt. %; low-Al— $\text{Al}_2\text{O}_3 < 1.5$ wt. %.

Regarding the nature of the network former, i.e., the use of high-purity sand or pure quartz, the heightened Zr content (29.1–334 ppm, avg. 138 ppm) of both black-appearing samples and white glass decorations could point to the use of sand, since Zr is often concentrated as zircon accessories in the heavy mineral fraction [81,85]. Similarly high Zr contents were detected in low-Al-high-Zr natron glass from SE Europe [62], and EIA (high-Zr) natron glass from Italy (FM4inc, AM1g, SN37t, SN35t, SN38t, NS32g, SN4t, SN7t, SN9g, SN3inc, SN33a, CA13inc) [22,84], with authors interpreting these values as indicative of the use sand [62], specifically of mature sands rich in quartz and zircon in the case of Italian samples [22,84], as opposed to pure quartz.

Nevertheless, it is important to stress that glasses known to have been made with sand, such as Hellenistic or Roman glass, commonly contain higher Al_2O_3 concentrations (>2 wt. %) and TiO_2 in variable amounts (0.05–0.5 wt. %) [9,13,56,63,64,69,86]. On the other hand, investigations of potential European glassmaking sands used in antiquity identified the deposits in Puglia (SE Italy) as sand suitable for glassmaking, with low Al_2O_3 content (1.1 wt. %) [81,87,88]. The possibility that pre-Roman glass was produced in Italy using local, low-Al sand has been proposed, but remains unconfirmed so far [20]. Earlier analyses of low-Al (<1 wt. % Al_2O_3) glassmaking sands exist for Egyptian deposits, notably the deposits at Achmounein (Tel el Ashmunein) and Alexandria [89], but the lack of trace element data precludes a more detailed comparison.

3.3.3. Stabilizer

In soda-lime-silica glass, calcium oxide is introduced to natron glass as calcite or shell impurities in the sand or as an intentionally added fraction. CaO values for the polished samples analysed by VP-SEM-EDS (7.8–9.9 wt. %), and the LA-ICP-MS data (1.9–10.0 wt. %, avg. 7.0 wt. %) fall within the typical range for Iron Age soda-lime-silica glass (Figure 6A) [12–14,20,22,35,62,80,84], with the exception of low CaO samples VC-16w (1.89 wt. %) and VC-110w (3.35 wt. %). The low levels of lime detected in these two samples could be related to their state of preservation. Although CaO values are within the expected range for natron glass, low MgO and Al₂O₃ concentrations result in overall lower stabilizer content of the studied samples as opposed to high-Al natron glass. The resulting relative depletion of stabilizing ions in the studied samples might explain the chemical susceptibility of black-appearing beads as opposed to other colours reported for the site [35]. Alumina substitutes for SiO₂ in the glass network, increasing the chemical durability, surface hardness, and mechanical endurance of glass [90]. While alumina content of black-appearing beads is lower than in the previously analysed samples from the site [35], their lime contents are comparable, meaning that the black-appearing beads are overall depleted in oxides which are known to increase the chemical durability of glass, mainly CaO* (avg. 7.66 wt. %), MgO* (avg. 0.45 wt. %) and Al₂O₃* (avg. 0.64 wt. %). The low alumina in black-appearing beads from Vinha das Calças 4 could therefore have contributed to the mechanism which rendered these beads prone to chemical attack [35]. A further argument in favour of this explanation could be the fact that white glass with lower FeO* (avg. 0.71 wt. %) appears more degraded than the black glass body in which the higher concentration of iron (avg. 4.09 wt. % FeO*) assumes the dual role of colourant and stabilizer [2]. A similar mechanism was previously argued for the precipitation of a corrosion layer on the bead surface of low-Al HMG glass from Świbie (Poland) [25].

Because calcium oxide can derive from various raw materials, a further examination of Ca-associated trace elements can offer insight into the nature of the stabilizer used. CaO/Sr ratios have been used as indicators of the source of lime [13–15,35,91] and, to an extent, as a discriminant between the use of coastal (mollusc-rich) or inland (mollusc-poor) silica sources since Sr in seawater is continuously incorporated into mollusc shells and aquatic microorganisms through biomineralization [92–94]. Low Sr values (<200 ppm) are associated with early Islamic (8th–9th c. AD) primary glass reworking at Tel el Ashmunein, Egypt, while high values (>300 ppm) are reported for Byzantine (6th–8th c. AD) primary production at Bet Eli'ezer and Bet She'an on the Levantine coast [91]. CaO/Sr ratios calculated for potential raw materials show that low ratios (212) can be expected if marine carbonates were present in the batch, and high ratios (870) if limestone is used as a stabilizer [94]. Consequently, low CaO/Sr ratios (<200) have been interpreted in the literature as evidence for the presence of fresh seashells in the glass batch (either added or present in coastal sand), whereas high CaO/Sr ratios (>600) are considered indicative of the use of inland deposits containing diagenetically altered limestone as a stabilizer [35,91,94]. Calculated CaO/Sr ratios for the analysed black (241–453, avg. 321) and white glass samples (263–652, avg. 385), are overall higher than those previously reported for the Levantine glass from Vinha das Calças 4 (161–215, avg. 189) [35], indicating the use of a different stabilizer type (Figure 6B), unlikely to have been sourced in coastal areas. Comparative datasets displaying similar behaviour of CaO/Sr ratios in Figure 6B include early natron glass from South Italy, interpreted as possible use of diagenetically altered shells [22], low-Al glass from SE Europe [62], and Mediterranean group III vessels from Adria (Italy) [13], thought to have been made with continental sand.

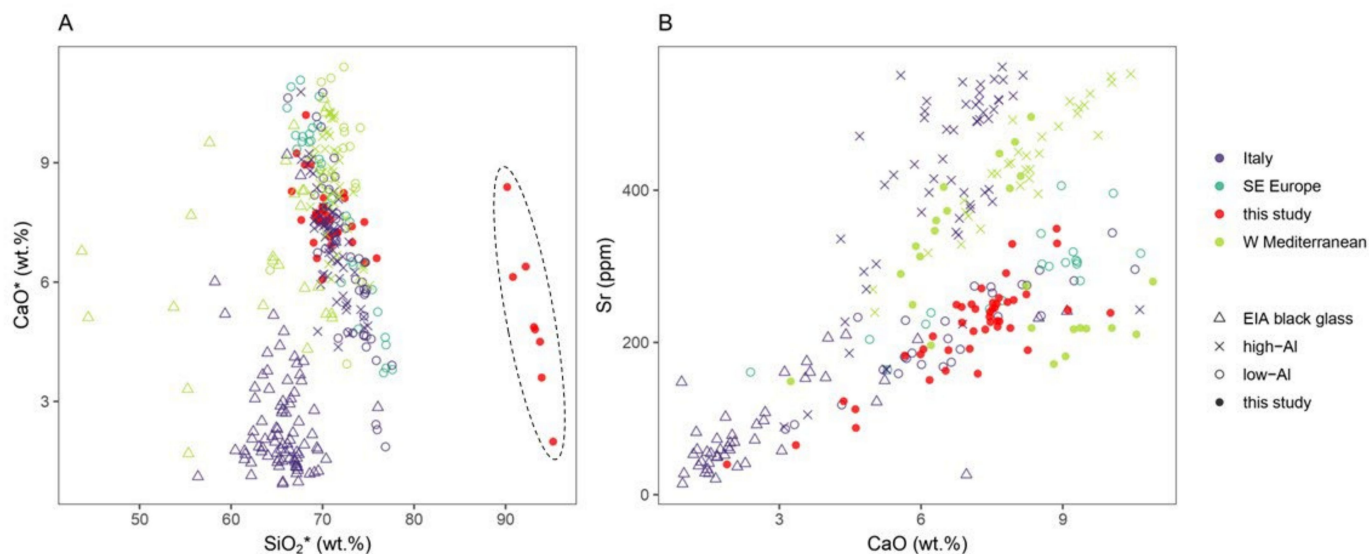


Figure 6. (A) $\text{CaO}^*/\text{SiO}_2^*$ biplot showing the differences and similarities in the lime content of black-appearing beads from Vinha das Calças 4 (this study, LA-ICP-MS data) and comparative Iron Age glass from various assemblages. Leaching in samples VC-16w, VC-26w, VC-28w, VC-77w, VC-109w, VC-110w and VC-141w (dashed ellipse) results in relative enrichment of SiO_2^* . (B) Sr/CaO biplot demonstrating different lime sources for black-appearing beads from Vinha das Calças 4 (this study, LA-ICP-MS data) and comparative Iron Age glass from various assemblages. CaO^* , SiO_2^* —values normalized to the sum of 8 oxides (Na_2O , MgO , Al_2O_3 , SiO_2 , K_2O , CaO , TiO_2 , FeO). Explanation of comparative dataset: Italy—natron and black glass beads from Sarno, Cumae, and Capua [22], black glass beads from Bologna, Pozzuoli and Cumae [14], natron and black glass beads from Francavilla Marittima, Torre Galli and Amendolara [84], Mediterranean Group I, II, III vessels from Adria [13], Mediterranean Group II vessels from Satricum [20]; SE Europe—low-Al natron glass beads from Una River Valley and Sanski Most (Bosnia and Herzegovina), Turska Kosa, Istria, Kompolje, Smiljan, Ljubač and Pannonia (Croatia) [62]; W Mediterranean—black glass beads from Carthage (Tunisia) [80], Levantine natron glass beads from Vinha das Calças 4 [35], natron glass from Son Mas (Mallorca, Spain) [12]; EIA black glass—soda-lime-silica samples reported as black glass [14,22,80]; high-Al— $\text{Al}_2\text{O}_3 > 1.5$ wt. %; low-Al— $\text{Al}_2\text{O}_3 < 1.5$ wt. %.

3.4. Colouring Technology

Compositional data for the analysed samples also allowed for the characterisation of the colouring technology employed in the production of black-appearing bead bodies and white glass decorations.

Thirty black-appearing glass samples can be characterised as Fe-coloured black-appearing glass since they feature heightened FeO concentrations (2.21–7.58 wt. %) relative to other colourants (Figure 7A). Notable amounts of Sb_2O_3 were detected in samples VC-24bl, VC-30bl, VC51bl, VC-94bl, VC-95bl, VC-96bl, VC-97bl, VC-129bl, and of PbO in samples VC-51bl, VC-95bl, VC-109bl, VC-115bl, VC-118bl and VC-129bl. One of the beads identified as a black-appearing bead during the visual examination, VC-81, is better characterised as Cu-Co blue, containing 0.68 wt. % CuO and 0.04 wt. % CoO, as well as low FeO (0.48 wt. %). Coupled with low Al_2O_3 content, the composition of sample VC-81 is drastically different from previously studied blue beads of Levantine origin from the site [35], indicating both a different glassmaking recipe and colouring technology employed in its production.

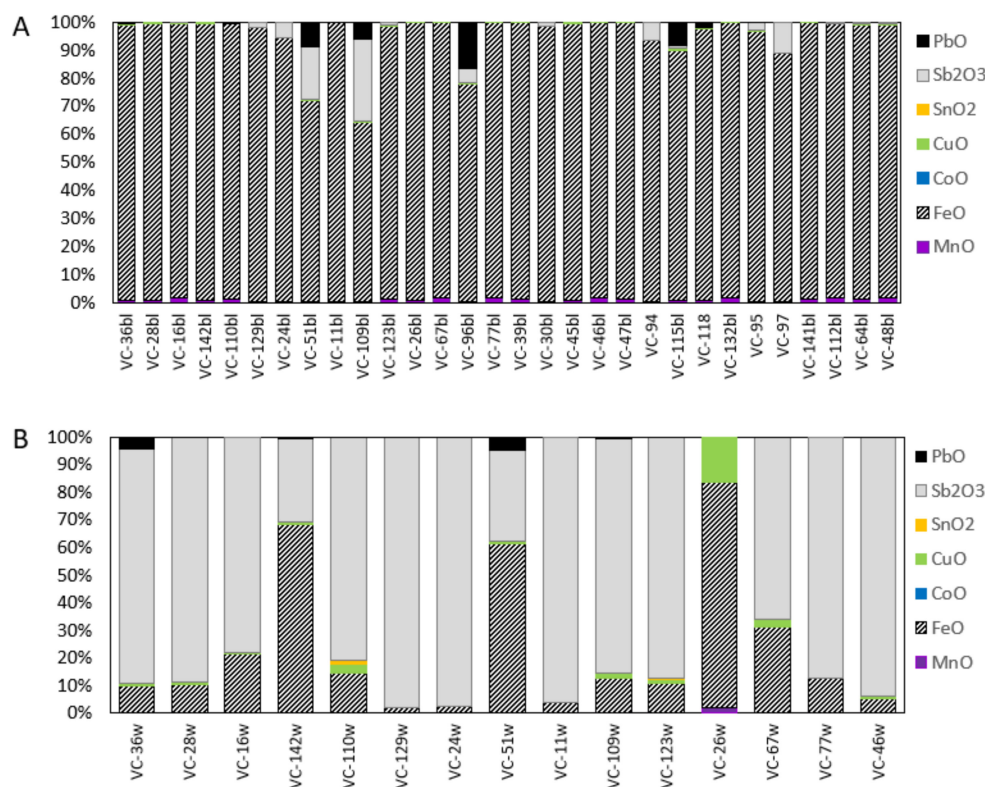


Figure 7. Relative content of selected colourant-related oxides (LA-ICP-MS data). (A) Black-appearing glass. The high content of FeO relative to other colouring oxides shows the colouring technology relied on the addition of iron to achieve the dark colouration. (B) White decorations. Relatively high amounts of Sb_2O_3 indicate that the colouring technology relied on the addition of calcium antimonate, with the exception of sample VC-26w.

The white colour of the bead decorations was achieved through the addition of a high amount of antimony relative to other colouring species (Figure 7B) and the formation of calcium antimonate opacifiers in the matrix. Exceptionally, the white colour of the decoration in the bead VC-26 was achieved by incorporating gaseous bubbles in the glass matrix. Iron-coloured back-appearing and antimonate-coloured white glass are further discussed below.

3.4.1. Black-Appearing Glass

Although glassmaking sands usually contain some naturally present iron, iron-rich sands might have intentionally been chosen for the production of EIA black glass [14]. In the black-appearing glass beads of Vinha das Calças 4, the iron content is higher than other non-black low-Al glass, suggesting iron was intentionally added as a colourant (Figure 5B). $FeO-Al_2O_3$ and $FeO-TiO_2$ ratios (>2.4 and >18 , respectively) are high and there is no strong correlation between iron and titania ($R^2 = -0.28$) or alumina ($R^2 = -0.2$), further illustrating that an iron-rich colourant might have been intentionally added to the base glass from Vinha das Calças 4.

The results of mineralogical and textural analysis of the black-appearing glass offer additional evidence for the intentional use of iron-based colourants. Analysis by μ -XRD revealed a single case of magnetite (Fe_3O_4) in the sample VC-67bl (Figure 8, Table S3—Supplementary Information), most likely corresponding to the iron inclusion observed by VP-SEM-EDS in the same sample (Figure 9A). Virtually identical inclusions of dendritic iron oxide were observed in the black-appearing samples VC-110bl, VC-129bl, and VC-132bl, (Figure 9). EDS analysis of these inclusions showed they are composed of iron oxide. Their composition and morphology match the iron inclusions observed in

black glass beads from the Tophet in Carthage (Tunisia) which have been interpreted as magnetite in the form of iron slags added to imported glass to produce the characteristic black colour [80]. Similar technology was likely employed to obtain the black-appearing colouration of the beads from Vinah das Caliças 4.

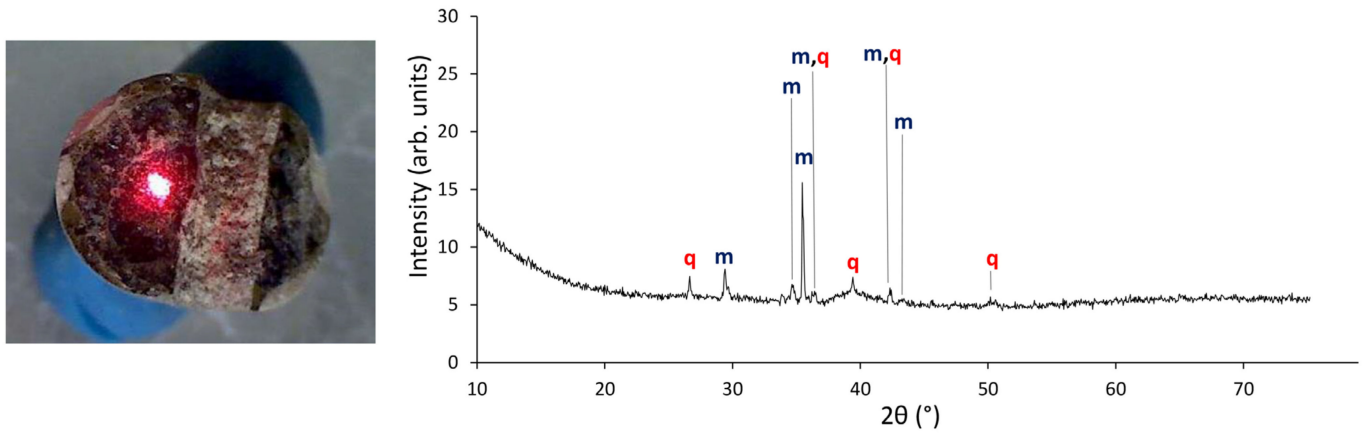


Figure 8. The analysed spot and the diffractogram of sample VC-67bl with identified crystalline phases: (m) magnetite, (q) quartz.

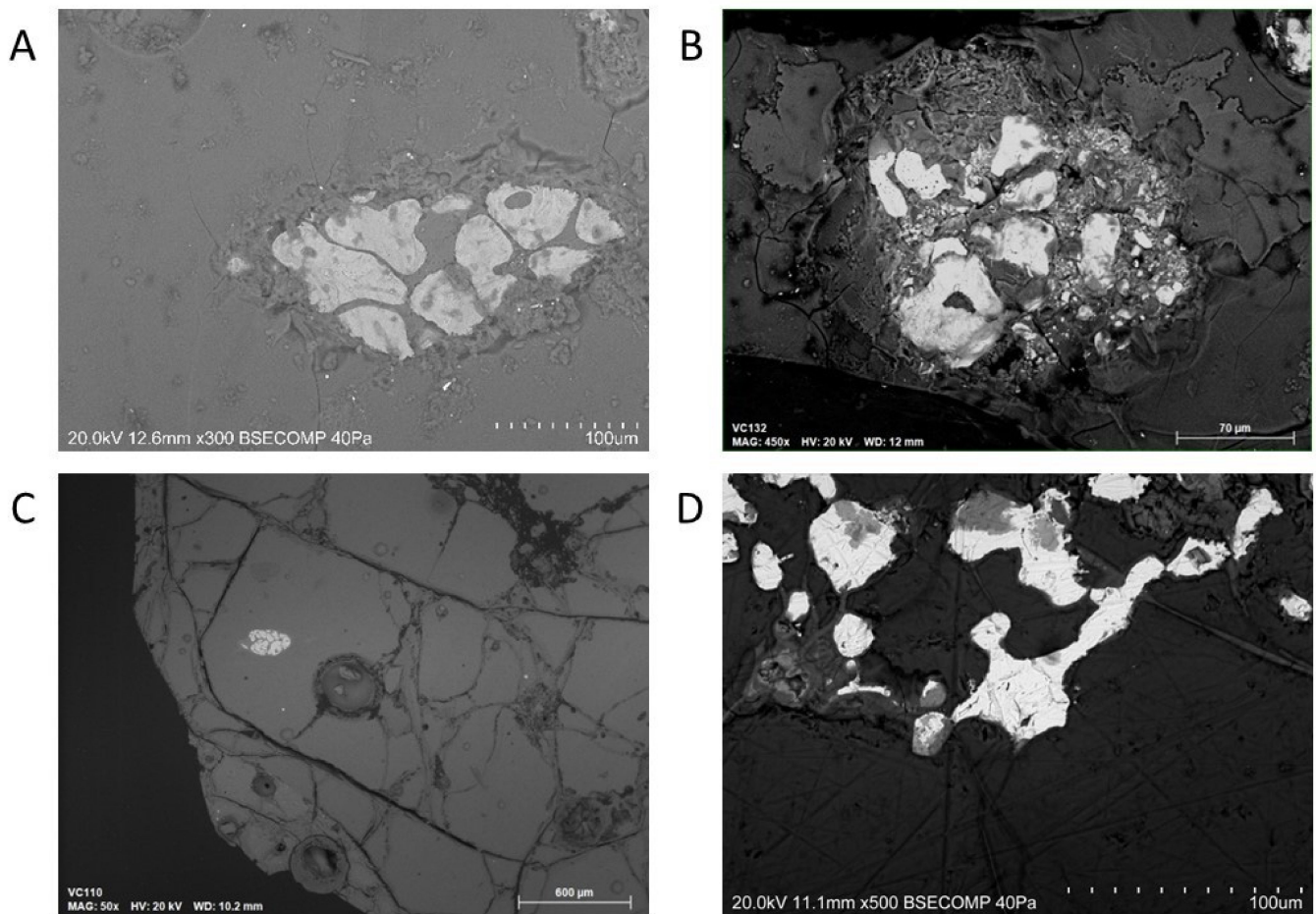


Figure 9. Iron inclusions observed by VP-SEM-EDS in the black-appearing glass beads from Vinha das Caliças 4: (A) VC-67bl; (B) VC-132bl; (C) VC-110 (polished section); (D) VC-129bl (polished section).

Moreover, four distinct colourant groups of black-appearing glass can be distinguished based on their iron contents, and Fe-associated elements like Al, Sb, Mn, Pb, and Ba (Figure 10, Table S4—Supplementary Information), suggesting a link between bead typology and colouring technology. Elevated concentrations of (de)colourant-related transition metals like Mn, Cu, Sn, Sb, and Pb can be indicative of the mixing (or recycling) of different glasses. These practices are well documented for Roman glass and the early medieval period [81,85,95–98] but less understood for periods prior to the Late Iron Age, when glassworking and the import of raw glass became a widespread phenomenon throughout Europe [17,18]. For Roman glass, intermediate amounts (ca. 100–1000 ppm) of colourant-related transition metals are taken as indicators of recycling or mixing or raw glass [95]. Aside from elevated concentrations, highly variable concentrations of transition metals can also be an indicator of glass mixing [98]. On the other hand, very high levels of transition metals in glass (>1000 ppm) are usually considered to result from intentional addition, rather than mixing and recycling of different glasses [81,85]. Discrete ranges of Sb, Mn, Ba, and Pb in the observed colourant groups (Figure 10, Table S4—Supplementary Information) suggest that the compositions of the four colourant groups result primarily from different colouring processes, rather than glass mixing or recycling. A notable exception would be the colourant Group 4, whose elevated and variable Mn and Sb content could suggest the mixing of different types of glass, in conjunction with the addition of a specific ingredient imparting high Pb and Ba to the final product. In this case, attempting to understand the final composition of each colourant group by looking at some element-specific associations could illuminate particular aspects of the *chaines opératoires* resulting in each of the black-appearing groups.

Group 1—high-Mn-Fe “black”—is represented by twelve samples. All beads of this group are beads with white decorations in a wavy line pattern. This group is characterised by a high FeO/Al₂O₃ ratio (8.24) and high FeO (avg. 4.27 wt. %). Mn content of this group is the highest among the analysed black-appearing beads (avg. 518 ppm), and these twelve samples also have an overall low Ba content (avg. 50.7 ppm). The lack of a strong Ba-Mn correlation ($R^2 = 0.24$) excludes the possibility that these two elements originate from the same ingredient. On the other hand, the Fe-Mn correlation is strong ($R^2 = 0.58$), suggesting at least some of the Mn in this group was introduced with the colourant. While MnO can be used to produce dark purple “black” glass, the reported contents for Roman Mn-black glass are much higher (>2 wt. %) than those detected in Group 1 [56,63,64]. Elevated Mn of Group 1 could also be explained by the use of manganese as a decolourant for the base glass prior to the addition of an iron-based colourant [99]. Although the use of Mn as a decolourant can be traced back to the Late Bronze Age glassmaking tradition [60], Mn-decolourised glass was rare prior to the Hellenistic period (5th c. BCE–1st c. BCE) [99]. Nonetheless, given the high Mn concentration, significantly above the ~200 ppm cutoff value for Mn-decolourised glass reported in the literature [99], and the lack of Ba-Mn correlation which would have suggested its addition as impurities in the silica source, it seems that the black-appearing glass of Group 1 could have been made by adding a colourant to a previously Mn-decolourised glass. The low alumina values and high FeO/Al₂O₃ ratio of the samples included in this group also point to the use of a silica source with a very limited amount of impurities. FeO shows a strong positive correlation with both Co ($R^2 = 0.64$) and Mn ($R^2 = 0.58$), which is a relationship characteristic of magnetite, and likely reflects its addition to the glass [100,101].

Group 2—mid-Mn-Fe “black”—consists of beads with “pseudo-eyes” made by looping a single strand of white glass. Alumina content of Group 2 is the highest of the black-appearing groups (Table 4), and when coupled with the generically elevated titania values (Table 4) and the low FeO/Al₂O₃ ratio (3.35) of these samples, could suggest the use of a comparatively less pure silica source in their manufacture. Ba is elevated in all the samples, in the 100–200 ppm range (avg. 129 ppm), while Mn is slightly higher (avg. 246.41), but comparable to Ba. Both elements are positively correlated ($R^2 = 0.55$), suggesting they were introduced with the same raw material, most likely as sand impurities. Based on iron and

manganese concentrations, Group 2 can further be split into 2 subgroups: (a) low iron subgroup ($\text{FeO} < 3$ wt. %, $\text{Mn} < 220$ ppm), and (b) high iron subgroup ($\text{FeO} > 3$ wt. %, $\text{Mn} > 260$ ppm) (Figure 10B).

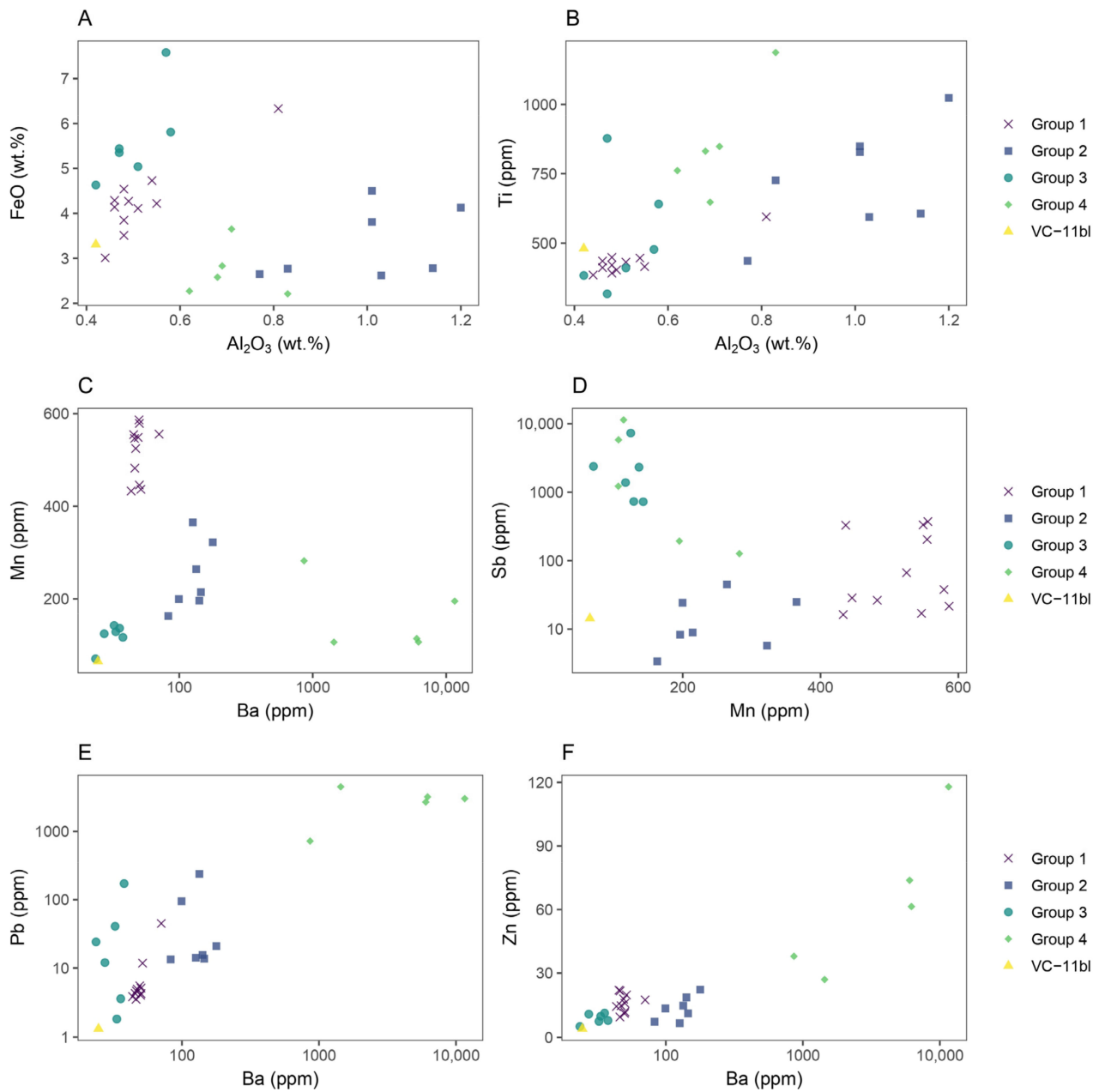


Figure 10. Biplots showing element associations in different black colourant groups from Vinha das Caliças 4. (A) FeO/Al₂O₃ biplot; (B) FeO/Mn biplot; (C) Mn/Ba biplot; (D) Sb/Mn biplot; (E) Pb/Ba biplot; (F) Zn/Ba biplot.

Table 4. Average major and minor oxide concentrations for the black-appearing colourant groups. All oxides expressed as wt. %. LA-ICP-MS data unless indicated otherwise (*).

	Decoration Type		Na ₂ O	MgO	Al ₂ O ₃	SiO ₂	P ₂ O ₅ *	SO ₃ *	Cl *	K ₂ O	CaO	TiO ₂	MnO	FeO	CoO	CuO	SnO ₂	Sb ₂ O ₃	PbO
black Group 1 (N = 12)	wavy line	avg	16.53	0.46	0.52	68.94	0.04	0.23	0.55	0.61	7.64	0.07	0.06	4.27	>0.01	0.01	>0.01	0.01	>0.01
		SD	0.36	0.05	0.10	1.04	0.08	0.22	0.37	0.12	0.25	0.01	0.01	0.83	>0.01	0.01	>0.01	0.02	>0.01
black Group 2 (N = 7)	"pseudo-eye"	avg	17.18	0.47	1.00	68.27	0.10	0.81	0.29	0.55	7.78	0.11	0.03	3.32	>0.01	0.02	>0.01	>0.01	>0.01
		SD	0.48	0.05	0.15	1.10	0.17	0.70	0.28	0.12	0.80	0.03	0.01	0.80	>0.01	0.01	>0.01	>0.01	0.01
black Group 3 (N = 6)	"eye"	avg	15.67	0.42	0.50	68.20	0.12	0.17	0.86	0.23	7.71	0.09	0.02	5.64	>0.01	>0.01	>0.01	0.33	>0.01
		SD	1.08	0.07	0.06	1.37	0.17	0.29	0.51	0.05	1.56	0.03	0.01	1.03	>0.01	>0.01	>0.01	0.33	0.01
black Group 4 (N = 5)	various	avg	16.63	0.44	0.71	69.43	0.05	0.48	0.60	0.42	7.18	0.13	0.02	2.71	>0.01	0.01	>0.01	0.39	0.27
		SD	0.94	0.06	0.08	1.46	0.11	0.16	0.19	0.05	0.47	0.04	0.01	0.58	>0.01	0.01	>0.01	0.51	0.14
outlier	other	VC-11bl	16.63	0.36	0.42	71.21	>0.01	0.55	>0.01	0.16	7.20	0.10	0.01	3.31	>0.01	>0.01	>0.01	>0.01	>0.01
		SD	-	-	-	-	-	-	-	-	-	-	-	-	-	-	-	-	-

* measured by VP-SEM-EDS.

Group 3—high-Sb-Fe “black”—is comprised of “eye” beads. Like Group 1, this group has a high FeO/Al₂O₃ ratio (11.2), and the iron content is slightly higher (5.64 wt. %) than that of the other groups. The Sb content of this group is very high (724–7311 ppm), meaning that it was most likely either a component deliberately added to the base glass, or an impurity in the colourant [56,64,81]. Ba and Mn levels are the lowest of all the groups (avg. 31.8 and 120 ppm, respectively). Both elements are strongly positively correlated ($R^2 = 0.67$). Coupled with their low concentrations, they could have been introduced as impurities naturally present in the silica source. Similar Mn, Ba, and Sb concentrations to those of Group 3 (“eye beads”) are reported for Fe-Co blue and colourless or weakly coloured low Al natron glass from Southeast European contexts [62], which could imply Group 3 was made by adding an iron colourant to the same base glass. It is also interesting to note that the low-Al samples Lj3b (Ljubač, Croatia) and SM66b (Sanski Most, Bosnia and Herzegovina), which exhibit FeO concentrations comparable to Group 3, are also “eye beads”, although their hue is listed as blue [62]. Co concentrations of these two samples, as well as of Group 3 samples are low (<53 ppm), and it is not clear what part they play in the colouring mechanism given the high amount of iron. It is worth noting that the Co and Ni contents of Group 3 are on average higher than that of the other black-appearing Groups (Table S4—Supplementary Information), which could imply Group 3 glass was originally coloured with a Co-bearing ingredient. While Co is a strong glass colourant known to impart a blue hue in concentrations as low as ~40 ppm [102,103], the polished fragments of samples VC-24bl and VC-129bl exhibit a green hue under transmitted light. Taking the high Sb content of both the low Al glass from SE Europe and the black-appearing Group 3 eye beads into account, it could be posited that this base glass was deliberately decoloured and later coloured with an iron-based colourant, either in different workshops across the Mediterranean, or somewhere in the glassmaking region. Alternatively, the elevated Co content could result from the use of a specific type of iron, such as magnetite, which can incorporate transition metals including Ti, Cr, Mn, Co, Ni and Zn [100,101]. In fact, Co-enriched iron particles interpreted as naturally present impurities in sand were documented in Egyptian faience beads from Vinha das Calças 4 [67]. The use of Sb as a decolourant in natron glass is attested throughout the 1st millennium BCE [8,15,17,25,99,104–106], and is, in fact, documented in the contemporary colourless beads of Levantine origin from Vinha das Calças 4 [35]. In this case, both Groups 1 (beads with wavy line decorations) and 3 (“eye” beads) might have been made using decolourised glass coming from (presumably) at least two workshops relying on starkly different decolourants.

Group 4—high-Pb-Ba “black”—includes samples VC-51bl, VC-96bl, VC-109bl, and VC-115bl. Represented types include beads with a wavy pattern and beads with “pseudo-eyes”. The group is not easily defined because of its highly heterogeneous compositions. This group has the lowest iron content (2.71 wt. %) and the FeO/Al₂O₃ ratio is low (3.87). However, compared to other colourant groups, Group 4 exhibits the highest Pb (722–2828 ppm) and Ba (861–115,586 ppm) contents, intermediate Mn (avg. 161 ppm), overall low FeO (2.71 wt. %), and variable Sb (126–11,385 ppm) levels. Samples VC-51bl, VC-109bl and VC-115bl also contain heightened levels of Zn (61.4–118 ppm). Extremely high Ba and Pb concentrations are probably a result of the intentional addition of the colourant, rather than the result of glass mixing. Ba and Mn are weakly negatively correlated ($R^2 = -0.15$), excluding the possibility that their concentrations result from the same ingredient. Sample VC-118 can also be considered within this group due to its similar Pb and Ba content, as well as trace and REE behaviour patterns. However, it is important to note that the Mn (282 ppm) and FeO (3.7 wt. %) levels of VC-118bl are somewhat higher compared to the rest of the Group 4 samples. Although heterogeneous, Group 4 stands out as particularly interesting due to its unusual composition. Comparable barium levels in Iron Age natron glass have seemingly only been recorded in black-appearing glass from Carthage Tophet [80], but were mostly found in the altered glass matrix of small, highly crystalline dark beads (glass type C) and correspond to the lower Ba range (>2000 ppm) of colourant Group 4. Since trace element data are not available for an in-depth comparison, highlighting some high-Pb samples (5588A, 6939A, 5598A, 3187A, 3187B, 3187C) can be used to establish another compositional parallel between the Carthage samples and the colourant Group 4 of black-appearing glass from Vinha das Calças 4. Barite inclusions were not observed by VP-SEM-EDS in the analysed samples and no Ba-containing inclusions were present in the LA-ICP-MS signal curve of the Group 4 samples, excluding the possibility that the Group 4 is an artefact resulting from sample heterogeneity. Similarly, to the interpretation of the local colouring and manufacture for the black-appearing glass from Carthage, group 4 black-appearing glass from Vinha das Calças 4 could represent a (so far) small-scale manufacture(s) reliant on mixing of available glass and colouring it with locally available colourants. The relationship between Ba, Pb, and Zn in Group 4 could, for instance, be indicative of the addition of lead slags to the glass. Lead slags are known to contain iron, barium, and zinc [57], and are usually associated with silver extraction [41,107–109]. Their use has been documented in the production of medieval lead glass [107,109,110], including high-Ba Umayyad (mid-8th c. CE–818 CE) lead glass from Saqunda (Cordoba, Spain) which was linked to the use of lead slags from silver-mining operations at Villanueva del Duque mines (Spain) by Pb isotope analysis [107]. Although there is a significant chronological and technological difference between medieval lead glass and Iron Age soda lime silica glass, silver extraction from Iberian lead ores has been confirmed as far back as the Iron Age [41,111], raising the possibility of waste material associated with Phoenician metallurgical activities like those attested in Carthage [112] being added, accidentally or on purpose, during secondary glass reworking.

Sample VC-11bl can be considered an outlier as it exhibits low levels of Ba, Mn, Pb, and Zn, similar to Group 3, but its low Sb content and somewhat lower FeO (3.3 wt. %) set it apart as a potentially fifth colourant.

3.4.2. White Glass

The white colour of the decorations was achieved predominantly by the addition of calcium antimonate acting as both colourant and opacifier, with Sb₂O₃ showing a wide range of values (1.4–10.6 wt. %) and corresponding to the relative amount of opacifiers observed in the glass texture (Figure 11). A single exception among the white decorations is sample VC-26w, in which the white appearance of the decoration was achieved by gaseous bubbles (Figure 12) in the glass matrix rather than the addition of antimonate opacifiers (<30 ppm Sb₂O₃). Unlike the black-appearing glass, different compositional groups cannot confidently be defined for the white glass due to the limited dataset and extensive leaching.

Reproducible measurements by LA-ICP-MS were only obtained for thirteen white glass samples (VC-11w, VC-16w, VC-26w, VC-28w, VC-46w, VC-48w, VC-51w, VC-77w, VC-109w, VC-110w, VC-129w, VC-141w), and only five samples (VC-11w, VC-46w, VC-48w, VC-51w, VC-129w) were reasonably well preserved ($\text{Na}_2\text{O} > 14$ wt. %).

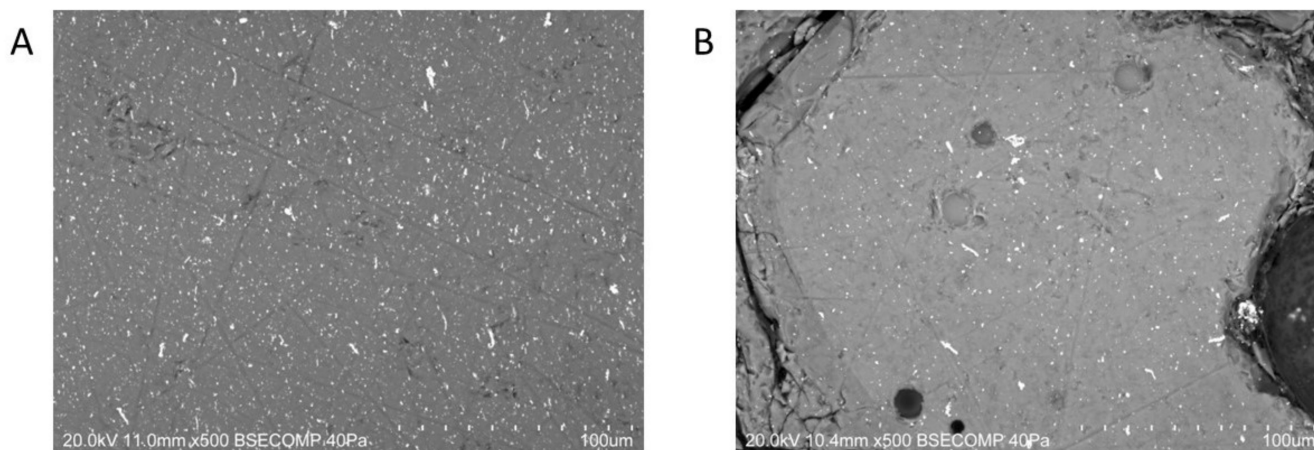


Figure 11. Examples of white glass textures characterised by different amounts of antimonate opacifiers observed by VP-SEM-EDS (BSE images). Note the heterogeneous size distributions of the aggregates and the elongated morphology in both textures. (A) VC-129w (10.6 wt. % Sb_2O_3) (B) VC-110w (4.6 wt. % Sb_2O_3).

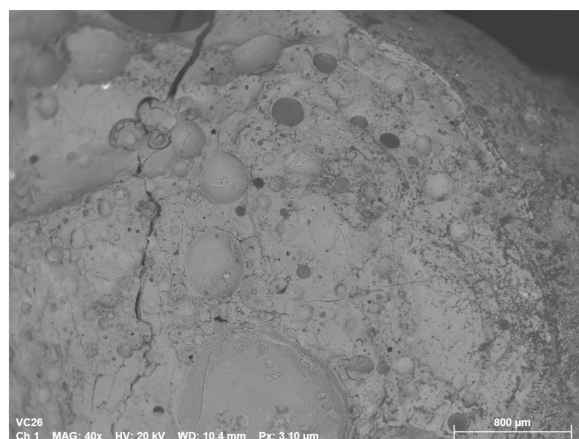


Figure 12. BSE image of the white glass decoration of bead VC-26. Note the absence of high-contrast opacifier crystals and the presence of bubbles in the matrix.

Calcium antimonate (CaSb_2O_6) was identified by μ -XRD in seventeen samples, primarily in white glass decorations (VC-16w, VC-24w, VC-30w, VC-46w, VC-47w, VC-48w, VC-51w, VC-94w, VC-112w, VC-115w, VC-123w, VC-129w, VC-132w) (Figure 13, Table S3—Supplementary Information). The few instances of the characteristic XRD patterns observed in black glass samples (VC-16bl, VC24bl, VC-123bl, VC-129bl) likely represent surface contamination during handling, since antimonate crystals were not observed in the texture of black glass (Figure 9). The textures of antimonate-opacified white glass samples are characterised by a homogenous distribution of opacifiers in the matrix. However, unlike the Levantine opaque glass from the site [35], the size distribution and morphology of individual aggregates in white glass of black-appearing beads could testify to a different opacification technique. Several works have suggested that the aggregate morphology of calcium antimonate can be used as an indicator of the opacification technique [35,113,114]. Elongated crystal aggregates documented in white glass decorations are reminiscent of rosary-shaped aggregates documented in Late Antique Roman white glass [115] linked to

an ex-situ opacification technique, i.e., the addition of previously synthesised antimonate to the glass. In line with the experimental studies of opacifier aggregate morphology [114], it could be argued that the elongated aggregates documented in the white decorations of black-appearing beads suggest an ex-situ opacification technique in which the previously synthesised opacifiers were added to the base glass, like in the 18th dynasty Egyptian (HMG) glass [113]. On the other hand, there does not appear to be a firm consensus on the link between aggregate morphology and the opacification technique so far [113–117]. It is also important to note that the current understanding between opacifier morphology and the opacification technique results from a relatively small number of targeted studies [113–117] which necessarily abstract the variability of actual conditions and materials used by ancient glassmakers.

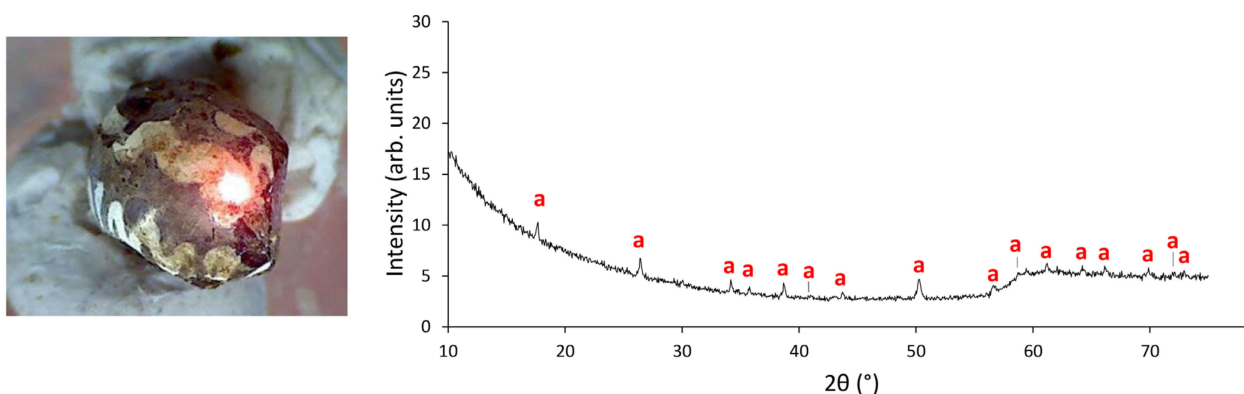


Figure 13. The analysed spot and the diffractogram of sample VC-51w with identified crystalline phases: (a) calcium antimonate (CaSb_2O_6).

All the samples contained exclusively hexagonal calcium antimonate (CaSb_2O_6) as opposed to the combination of hexagonal and orthorhombic ($\text{Ca}_2\text{Sb}_2\text{O}_7$) calcium antimonate. The singular presence of hexagonal calcium antimonate detected by μ -XRD stands in stark contrast to previously analysed opaque (Levantine) glasses from the site [35,53], further illustrating different technological conditions, possibly involving a relatively short, high-temperature regime [115].

3.5. Silica Sources

Aside from common sand impurities like alumina, trace elements related to accessory minerals in the silica source are indispensable for an in-depth characterisation of raw materials and understanding their provenance. In particular, trace elements related to heavy-mineral present in glassmaking sands are considered good discriminants of Egyptian vs. Levantine/Syro-Palestinian silica sources [12,15,17,18,35,118]. The zirconium content of the glass is thought to be a good indicator of the geological provenance of the silica source, regardless of whether the glassmaking technology relied on the use of pure quartz [119], or quartz sand as the source of network former [12,18,22,35]. Elements which substitute for Zr in zircons, like Nd or Hf, are also useful in silica provenancing [20]. Many natron glasses dating from the Iron Age to the late Antiquity/Early Medieval period show a remarkable similarity in their trace element patterns. Low Zr and high Sr and Ba values in natron glass are typically interpreted as originating in the Levantine region, based on the analyses of sand from the Belus River [81] and Levantine raw glass from Bet Eli'ezer and Apollonia [120]. On the other hand, glass from the 8th–9th c. CE Egyptian workshop at Tell-el-Ashmounein [120], as well as Celtic, Roman and Islamic natron glasses of Egyptian origin, are typically characterised by high Zr and low Sr contents [17,69,121]. Other trace elements mostly introduced to the glass through silica sources include Ti, V, Rb, Y, Ba, REE, Ta, Th, and, to an extent, U [81,85]. While Sr is more closely influenced by the stabilizer, rather than silica, it is considered among trace elements indicative of silica sources in this study because lime could have been naturally present in the glassmaking sand.

Trace element patterns of the analysed glass from Vinha das Calças 4 normalised to the composition of the Upper Continental Crust [122] are illustrated in Figure 14. The samples are divided according to similar trace element behaviour into “high Sr”, “high Zr”, “low Zr”, “high Sr-Ba”, and “high Ba” groups, based on the most noticeable difference in Sr-Ba-Zr relationship (Figure 14).

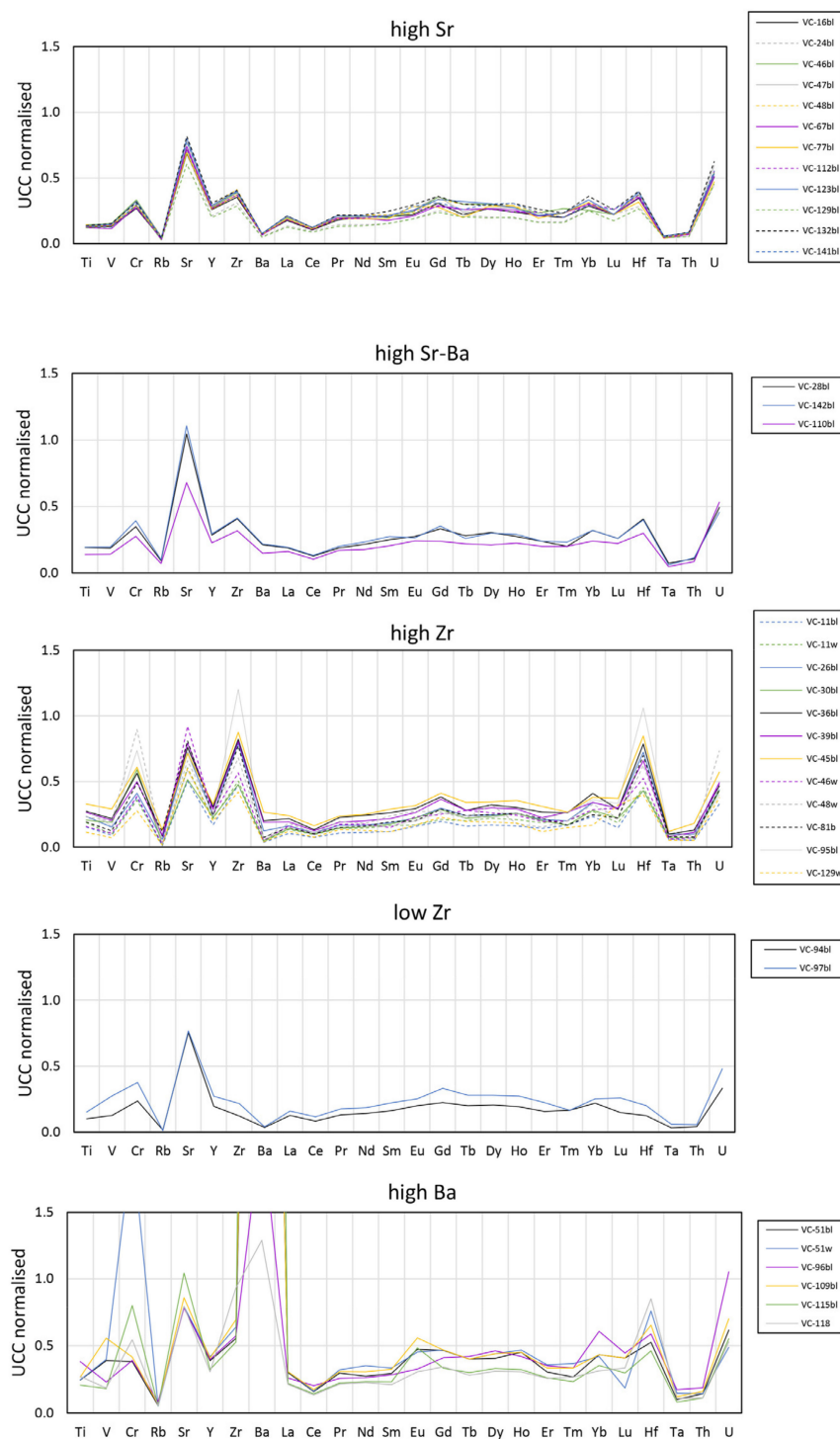


Figure 14. Trace element patterns of the black-appearing glass beads from Vinha das Calças 4. Values obtained by LA-ICP-MS and normalised to the Upper Continental Crust [122]. Leached samples VC-16w, VC-26w, VC-28w, VC77w, VC-109w, VC-110w, VC-123w, VC-141w (Table S1—Supplementary Information) not plotted.

Samples VC-16bl, VC-24bl, VC-46bl, VC-47bl, VC-48bl, VC-67bl, VC-77bl, VC-112bl, VC-123bl, VC-129bl, VC-132bl, and VC-141bl (“high Sr”) present a relatively uniform trace and REE pattern group characterised by elevated Sr (avg. 235 ppm) in relation to Zr (avg. 91.2 ppm), low Ba (avg. 47.7 ppm) and Cr (avg. 10.7 ppm), and a slight negative Ce anomaly. The three samples (VC-28bl, VC-142bl, VC-110bl) of the “high Sr-Ba” group behave similarly to the “high Sr” patterns but have a somewhat elevated Ba content (128.65 ppm) which could be ascribed to minor variations in the same silica source since the REE patterns of the two groups do not display marked differences, barring the smoother pattern of sample VC-110bl. Samples VC-11bl, VC-11w, VC-26bl, VC-30bl, VC-36bl, VC-39bl, VC-45bl, VC-46w, VC-48w, VC-81b, VC-95bl, VC-129w belonging to the “high Zr” group, exhibit some of the highest Zr levels (avg. 166 ppm) among the studied beads, comparable to their Sr contents (avg. 216 ppm). Relatively elevated Cr (avg. 18.1 ppm) in relation to Sr of this group could also be considered an attribute of the silica source, rather than the iron colourant, as white and blue glass samples VC-48w and VC-81b of this group contain more Cr (31.3 ppm and 17.1 ppm, respectively) than black glass in the “high Sr” (<14 ppm) and “high Sr-Ba” groups (Table S5—Supplementary Information). Ba contents (avg. 66.8 ppm) fall within the ranges for the “high Sr” and “high Sr-Ba” groups. Coupled with the similar REE patterns of the three groups, it could be taken to indicate a common source of silica, with compositions varying slightly between prepared glass batches or on a geologically local scale. Two black-appearing samples, VC-94bl and VC-97bl, are characterised by low Zr values (29.1 ppm and 51.4 ppm, respectively) more similar to Mediterranean coastal sands [13,91,120], although their Sr (239 ppm and 242 ppm) and Ba (23.6 ppm and 27.6 ppm) contents are significantly lower than the Sr and Ba contents of coastal sands. The “high Ba” group consists of six samples (VC-51bl, VC-51w, VC-96bl, VC-109bl, VC-115bl, VC-118) and corresponds to the Group 4 iron colourant. The trace element composition of this group is rather heterogeneous and slightly elevated compared to the other four groups, but common characteristics shared with most of the analysed samples include similar Rb, Sr, Y, Zr, Hf, Ta, Th and U behaviour, and a negative Ce anomaly. The positive Eu anomalies in the “high Ba” samples VC-115bl and VC-109bl further set these three samples apart from the rest of the analysed beads. Considering no other samples exhibit a noticeably positive Eu anomaly, the peculiar behaviour of these two samples could be influenced by the colouring technology via the same mechanism that impacts Ba and Sr levels, rather than the silica source. Continental barites, aside from occurring in association with galena (PbS), chalcopyrite (CuFeS₂), and sphalerite (ZnS), also show positive Eu anomalies [66]. In other words, the positive Eu anomaly might have resulted from the introduction of the same low-grade iron or lead slags used to colour the three samples. On the other hand, it is worth pointing out that trace element patterns of some archaeological glasses from Carthage are characterised by high Ba and Zr, as well as high Sr [120], which might prove to be indicative of a yet unidentified silica source, possibly along the North African coast.

The Zr values of analysed beads (99.6–334, avg. 168 ppm, with the exceptions of VC94bl and VC97bl) are overall higher than those recorded in the previously published blue, colourless, turquoise, yellow, and white beads from Vinha das Calças 4 [35]. These values are also higher than those reported for Eastern Mediterranean coastal sands (<ca. 74 ppm Zr or 100 ppm ZrO) and more evocative of the Zr content of Egyptian glass or glass made from inland sands reported in the literature [12,13,17,91,120,121,123]. The studied beads also differ drastically in their Ba/Sr and Zr/Sr ratios (Figure 15) from the Levantine beads from Vinha das Calças 4 [35], plotting more closely to low-Al natron glass from SE Europe [62], some natron glasses from Italy [22,84], Egyptian glass from Mallorca [12], and the low-Al Mediterranean Group II vessels from Satricum (Satricum A) [20]. A clearer distinction between the low-Al natron glass assemblages can be seen in Y and Ce concentrations (Figure 16), which group along three different trends (Figure 16), with the “high Sr”, “high Sr-Ba”, “high Zr”, and “high Ba” black-appearing beads showing more affinity to low-Al natron glass from Italy [22,84] and SE Europe [62] than the glass from Son Mas [12] and Satricum A [20] samples. It is interesting to note that an Egyptian origin was proposed

for the Italian natron glasses, the Son Mas samples, and the low-Al glass from SE Europe, while the Group A glasses from Satricum were not attributed to a specific silica source. The slight difference between these assemblages could point to the existence of multiple primary workshops in the geologically common glassmaking region, or the use of a less homogenous silica source. Based on the presented trace element data, a common, possibly Egyptian, geological origin for the black-appearing Iron Age glass beads and the majority of other Iron Age low-Al glasses is proposed.

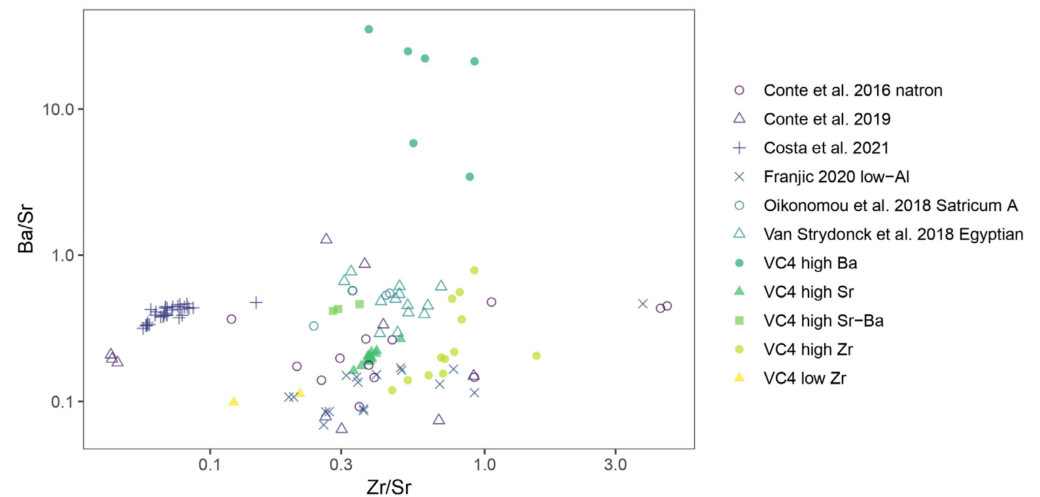


Figure 15. Ba/Sr vs. Zr/Sr biplot for the black-appearing beads from Vinha das Calças 4 and comparative Iron Age glass from various assemblages. Leached samples not plotted. Explanation of comparative dataset: Conte et al. 2016—natron glass beads from Sarno and Capua (Italy) [22]; Conte et al. 2019—natron glass beads from Francavilla Marittima, Torre Galli and Amendolara [84]; Costa et al. 2021—Levantine natron glass beads from Vinha das Calças 4 [35]; Franjic 2020—low-Al natron glass beads from Sanski Most (Bosnia and Herzegovina), Turska Kosa, Istria, Kompolje, Smiljan, Ljubač and Pannonia (Croatia) [62]; Oikonomou et al. 2018 Satricum A—“Satricum A” compositional group of Mediterranean Group II vessels from Satricum (Italy) [20]; Van Strydonck et al. 2018 Egyptian—natron glass from Son Mas (Mallorca, Spain) of Egyptian origin [12].

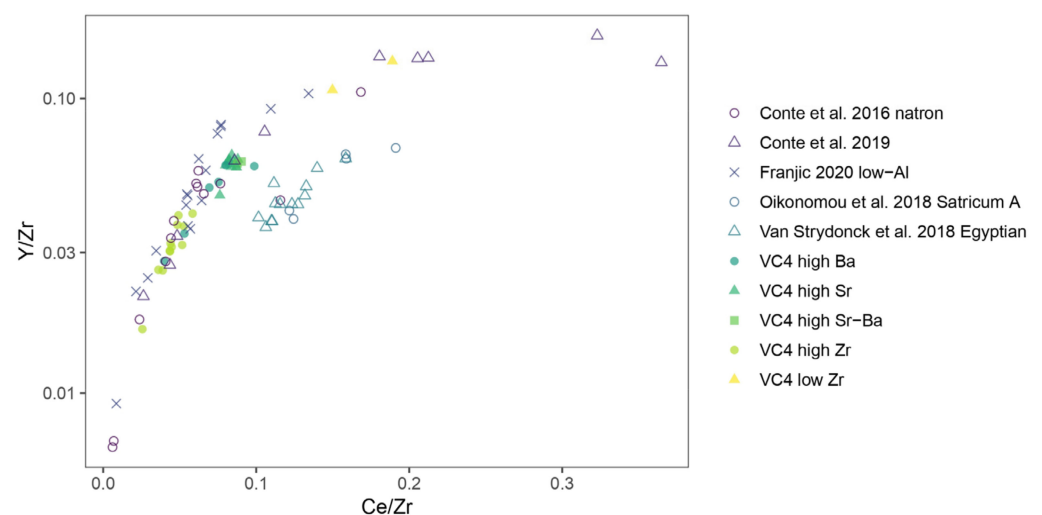


Figure 16. Y/Zr vs. Ce/Zr biplot for the black-appearing beads from Vinha das Calças 4 and comparative Iron Age glass from various assemblages. Leached samples not plotted. Explanation of comparative dataset: Conte et al. 2016—natron glass beads from Sarno and Capua (Italy) [22]; Conte et al. 2019—natron glass beads from Francavilla Marittima, Torre Galli and Amendolara [84];

Franjic 2020—low-Al natron glass beads from Sanski Most (Bosnia and Herzegovina), Turska Kosa, Istria, Kompolje, Smiljan, Ljubač and Pannonia (Croatia) [62]; Oikonomou et al. 2018 Satricum A—“Satricum A” compositional group of Mediterranean Group II vessels from Satricum (Italy) [20]; Van Strydonck et al. 2018 Egyptian—natron glass from Son Mas (Mallorca, Spain) of Egyptian origin [12].

4. Final Remarks and Implications for the Understanding of Iron Age Glass Trade Networks in the Mediterranean

Typological and compositional links between the black-appearing beads from Vinha das Calças 4 and other Iron Age glass assemblages from the Mediterranean explored in this work indicate that the presented set of black-appearing beads is a result of a complex network of primary glassmaking centre(s), secondary colouring workshops, and an uncertain number of beadmaking workshops situated in Phoenician-mediated Mediterranean trade networks. The major and minor oxide content of the samples is different from early natron glasses with low Ca, like EIA black glass, or Al-Co blue glass, and corresponds to low-Al natron glass, which is a less represented type of glass during the Early and Late Iron Ages [12,13,17,20,22,62]. Trace elements related to the silica source show more similarities with Iron Age glass interpreted as being of Egyptian provenance, as exemplified by their Zr, Sr, Ti and REE behaviour, suggesting that the base glass used in bead manufacture was produced in this, or a geochemically similar region. Distinct colourant groups detected among the black-appearing glass samples, however, point to different episodes of colouring, and the link between bead typology and colourant might suggest the existence of at least four workshops, one of which (Group 4) could have been an “amateur” workshop relying on low-grade colourants and imported, possibly mixed glass, to recreate bead types circulating in the Western Mediterranean.

The following observations on black-appearing Iron Age glass from the Iberian Peninsula might be considered useful in future Phoenician and Western Mediterranean studies. Firstly, the primary production centre(s) for the majority of the black-appearing glass considered here relied on a different glassmaking recipe and raw material sources than the centre which produced the blue, colourless, turquoise, yellow and white beads discovered at Vinha das Calças 4 and was most likely not located along the Levantine coast, as evidenced by the different major, minor, and trace element compositions between the two datasets. Secondly, the presented beads form a subset of a larger, but less common, IA compositional group, recently referred to as “low-Al glass” [62] that was in circulation throughout most of the 1st millennium BCE [1,12,17,20]. Based on the parallels with the Egyptian high-Zr beads from Mallorca (Spain) [12], Satricum A Hellenistic glass from Italy [20], Mediterranean II vessels from Adria (Italy) [13], early natron glass from Italy [22,84], and low-Al natron glass from SE Europe [62], the primary production region for this group could be located in Egypt or possibly a non-confirmed geochemically similar region, like South Italy or the North African coast. Egyptian workshops could be a good candidate for the origin of low-Al black-appearing beads, since other Egyptian imports like scarab amulets, faience beads, and Egyptian blue (cuprorivaite) frit were also discovered at Vinha das Calças 4 [14,16,18], but further studies on Egyptian glassmaking sands are needed. Finally, the colouring technologies employed for the black-appearing glass are different from the early IA black glass, including black natron glass (9th–7th c. BCE) [14,22,84], and more similar to the black glass from Carthage [80]. Moreover, there appears to be a strong link between bead typology and the colouring technology, suggesting the studied beads were produced in several beadmaking workshops employing iron colourants of different origins, or at least in several chronological instances in which different colourants were used. Textural and compositional similarity to black beads from Carthage [80], and the apparent limited distribution of this type of glass could imply that Eastern Mediterranean raw glass was reworked in the West to suit the local demands, particularly in relation to “eye” beads (Group 3) and Group 4 which mimics other types but uses an apparently less pure iron colourant, in addition to using glass from different workshops. Alternatively, the

beads could have been manufactured close to the primary production centre and traded as a finished product. If the latter is true, and with the caveat of a limited dataset from a single site, the typological–compositional link between Levantine beads [35] and low-Al black-appearing glass in Portugal (this study) could suggest that the trade networks in the Western Mediterranean were colour-coded to some extent, with different workshops supplying specific products and colour palettes.

The results presented here were obtained on a limited dataset from a single site. As such, they cannot be considered representative of the reality of the black-appearing glass phenomenon in Southern Portugal. Nonetheless, the conclusions regarding the production technology, origin of the raw materials, and distribution patterns reached through a compositional and textural study of black-appearing beads from Vinha das Caliças 4 allow us to put forth a set of working hypotheses to be tested in future studies of this peculiar phenomenon:

1. Black-appearing beads from Southern Portugal are (predominately) low-Al natron glass coloured with iron;
2. Trace element and REE related to the silica source show more similarities with glasses thought to have been produced in Egypt, than other known glassmaking regions in the (wider) Mediterranean;
3. Different iron colourants, were consistently used in the production of black-appearing beads;
4. There is a link between bead typology and the type of iron colourant used.

Supplementary Materials: The following supporting information can be downloaded at: <https://www.mdpi.com/article/10.3390/heritage7030061/s1>, Table S1: Results of LA-ICP-MS analyses of NIST610 (n = 60) and NIST612 (n = 36) reference materials, including average measured values (ppm), standard deviations (ppm), RSD (%) and RD (%) calculated after D’Oriano et al. [124], minimum estimated detection limits (DL), and recovery rates relative to certified values [125]. Certified values reported from Pearce et al., 1997 [125]; Table S2: VP-SEM-EDS measurements of the analysed black-appearing beads. All results normalised to sum of oxides. * polished samples; Table S3: Crystalline phases identified by μ -XRD; Table S4: Average trace element concentrations (in ppm) for the four black-appearing colourant groups. LA-ICP-MS measurements; Table S5: Trace and REE element concentrations of the analysed samples (LA-ICP-MS data).

Author Contributions: Conceptualization, V.L. and M.C.; methodology, M.C. and P.B.; validation, V.L. and M.C.; formal analysis, V.L.; investigation, V.L.; resources, A.M.A.; data curation, V.L.; writing—original draft preparation, V.L.; writing—review and editing, M.C. and A.M.A.; visualization, V.L.; supervision, M.C.; project administration, M.C.; funding acquisition, V.L. and M.C. All authors have read and agreed to the published version of the manuscript.

Funding: This research was funded by Fundação para Ciência e a Tecnologia–FCT, grant numbers EXPL/HAR-ARQ/0381/2021 (doi: 10.54499/EXPL/HAR-ARQ/0381/2021), UIDB/04449/2020 (doi: 10.54499/UIDB/04449/2020), UIDP/04449/2020 (doi: 10.54499/UIDP/04449/2020), LA/P/0132/2020 (doi: 10.54499/LA/P/0132/2020) and 2023.03646.BD, and the European Audiovisual and Culture Executive Agency–EACEA (EMJMD ARCHMAT programme), grant number 599247-EPP-1-2018-1-PT-EPPKA1-JMD-MOB.

Data Availability Statement: Data is contained within the article or Supplementary Materials.

Acknowledgments: The authors would also like to thank Arqueo Hoje for providing access to the archaeological artifacts.

Conflicts of Interest: The authors declare no conflict of interest.

Notes

- 1 For other possible sources of natron glass in the 1st millennium BCE, see references [20,21]. For 1st millennium BCE glass other than mineral soda-lime-silica (natron glass), see references [14,22–25].
- 2 “Phoenicians” is an ethnonym taken from the ancient Greek to designate the people inhabiting Levantine city-states like Tyre, Byblos, and Sidon. During the 1st millennium BCE, these cities saw a rapid colonial expansion across the Mediterranean and established a wide-spread network of maritime trade and production of luxury goods like dyes, textiles, and glass. There is, however, little evidence for their cultural, political, linguistic or religious centralisation. For further discussion, see references [26–31].
- 3 A full morphometric and typological study of the assemblage is underway. So far, 77 occurrences of beads with one or more wavy line decorations were documented in a set of 133 beads initially described as black-appearing.
- 4 28 occurrences among 133 observed black-appearing beads.
- 5 Diameter, measured as the largest perceived dimension of the bead when the apex (perforation) of the bead is observed.
- 6 19 occurrences among 133 observed black-appearing beads.

References

1. Gratuze, B. Les premiers verres au natron retrouvés en Europe occidentale: Composition chimique et chronotypologie. In *Annales du 17^e Congrès de l'Association Internationale pour l'Histoire du Verre/Annales of the 17th Congress of the International Association for the History of Glass*; Janssens, K., Degryse, P., Cosyns, P., Caen, J., Dack, L.V., Eds.; Antwerp University Press: Antwerp, Belgium, 2009; pp. 8–14, 47–54.
2. Reade, W.; Freestone, I.; Bourke, S. Innovation and continuity in Bronze and Iron Age glass from Pella in Jordan. In *Annales 17^e Congrès de l'Association Internationale pour l'Histoire du Verre. Annales of the 17th Congress of the International Association for the History of Glass*; Janssens, K., Degryse, P., Cosyns, P., Caen, J., Dack, L.V., Eds.; University Press Antwerp: Antwerp, Belgium, 2009; pp. 47–54.
3. Gomes, F.B. Early Iron Age “black” Glass in Southwestern Iberia: Typology, Distribution and Context. *Zephyrus* **2021**, *87*, 125–144. [[CrossRef](#)]
4. Henderson, J. Electron Probe Microanalysis of Mixed-Alkali Glasses. *Archaeometry* **1988**, *30*, 77–91. [[CrossRef](#)]
5. Rehren, T.; Rosenow, D. Three Millennia of Egyptian Glassmaking. In *Mobile Technologies in the Ancient Sahara and Beyond*; Duckworth, C., Cuénod, A., Mattingly, D., Eds.; Cambridge University Press: Cambridge, UK, 2020; pp. 423–450.
6. Schlick-Nolte, B.; Werthmann, R. Glass Vessels from the Burial of Nesikhons. *J. Glass Stud.* **2003**, *45*, 11–34.
7. Dardeniz, G. Was Ancient Egypt the Only Supplier of Natron? *New Res. Reveals Major Anatol. Depos. Anatolica* **2015**, *41*, 191–202.
8. Brill, R.H. *Chemical Analyses of Early Glasses; Tables of Analyses*; Corning Museum of Glass: Corning, NY, USA, 1999; Volume 2.
9. Arletti, R.; Ferrari, D.; Vezzalini, G. Pre-Roman Glass from Mozia (Sicily-Italy): The First Archaeometrical Data. *J. Archaeol. Sci.* **2012**, *39*, 3396–3401. [[CrossRef](#)]
10. Arletti, R.; Maiorano, C.; Ferrari, D.; Vezzalini, G.; Quartieri, S. The First Archaeometric Data on Polychrome Iron Age Glass from Sites Located in Northern Italy. *J. Archaeol. Sci.* **2010**, *37*, 703–712. [[CrossRef](#)]
11. Arletti, R.; Rivi, L.; Ferrarri, D.; Vezzalini, G. The Mediterranean Group II: Analyses of Vessels from Etruscan Contexts in Northern Italy. *J. Archaeol. Sci.* **2011**, *38*, 2094–2100. [[CrossRef](#)]
12. Van Strydonck, M.; Gratuze, B.; Rolland, J.; De Mulder, G. An Archaeometric Study of Some Pre-Roman Glass Beads from Son Mas (Mallorca, Spain). *J. Archaeol. Sci. Rep.* **2018**, *17*, 491–499. [[CrossRef](#)]
13. Panighello, S.; Orsega, E.F.; Elteren, J.T.; Šelih, V. Analysis of Polychrome Iron Age Glass Vessels from Mediterranean I, II and III Groups by LA-ICP-MS. *J. Archaeol. Sci.* **2012**, *39*, 2945–2955. [[CrossRef](#)]
14. Conte, S.; Arletti, R.; Henderson, J.; Degryse, P.; Blomme, A. Different Glassmaking Technologies in the Production of Iron Age Black Glass from Italy and Slovakia. *Archaeol. Anthropol. Sci.* **2018**, *10*, 503–521. [[CrossRef](#)]
15. Blomme, A.; Degryse, P.; Dotsika, E.; Ingnatiadou, D.; Longinelli, A.; Silvestri, A. Provenance of Polychrome and Colourless 8th–4th Century BC Glass from Pieria, Greece: A Chemical and Isotopic Approach. *J. Archaeol. Sci.* **2017**, *78*, 134–146. [[CrossRef](#)]
16. Shortland, A.J.; Schroeder, H. Analysis of First Millennium BC Glass Vessels and Beads from the Pichvnari Necropolis, Georgia. *Archaeometry* **2009**, *51*, 947–965. [[CrossRef](#)]
17. Rolland, J. *Le Verre de l'Europe Celtique. Approches Archéométriques, Technologiques et Sociales d'un Artisanat Du Prestige Au Second Âge Du Fer*; Sidestone Press: Leiden, The Netherlands, 2021; ISBN 978-90-8890-995-5.
18. Rolland, J.; Venclová, N. Iron Age Glass-working in Moravia, Central Europe: New Archaeometric Research on Raw Glass and Waste—3rd–First Century BC. *Archaeol. Anthropol. Sci.* **2021**, *13*, 124. [[CrossRef](#)]
19. Šmit, Ž.; Laharnar, B.; Turk, P. Analysis of Prehistoric Glass from Slovenia. *J. Archaeol. Sci. Rep.* **2020**, *29*, 102114. [[CrossRef](#)]
20. Oikonomou, A.; Henderson, J.; Gnade, M.; Chenery, S.; Zacharias, N. An Archaeometric Study of Hellenistic Glass Vessels: Evidence for Multiple Sources. *Archaeol. Anthropol. Sci.* **2018**, *10*, 97–110. [[CrossRef](#)]
21. Ham-Meert, A.; Dillis, S.; Blomme, A.; Cahill, N.; Claeys, P.; Elsen, J.; Eremin, K.; Gerdes, A.; Steuwe, C.; Roeffaers, M.; et al. A unique recipe for glass beads at Iron Age Sardis. *J. Archaeol. Sci.* **2019**, *108*, 109474. [[CrossRef](#)]

22. Conte, S.; Arletti, R.; Mermati, F.; Gratuze, B. Unravelling the Iron Age Glass Trade in Southern Italy: The First Trace-Element Analyses. *Eur. J. Mineral.* **2016**, *28*, 409–433. [[CrossRef](#)]
23. Tzankova, N.; Mihaylov, P. Chemical Characterization of Glass Beads from the Necropolis of DrenDelyan (6th–4th Century BC), Southwest Bulgaria. *Geol. Balc.* **2019**, *48*, 31–50. [[CrossRef](#)]
24. Schmidt, K. *Glass and Glass Production in the Near East during the Iron Age: Evidence from Objects, Texts and Chemical Analysis*; Archaeopress Publishing Ltd.: Oxford, UK, 2019; ISBN 978-1-78969-155-9.
25. Purowski, T.; Syta, O.; Wagner, B. Between East and West: Glass Beads from the Eighth to Third Centuries Bce from Poland. *Archaeometry* **2020**, *62*, 752–773. [[CrossRef](#)]
26. Quinn, J. *Search for the Phoenicians*; Princeton University Press: Princeton, NJ, USA, 2018; ISBN 978-0-691-17527-0.
27. Aubet, M.E. Phoenicians Abroad: From Merchant Venturers to Colonists. In *Eurasia at the Dawn of History: Urbanization and Social Change*; Krausse, D., Fernández-Götz, M., Eds.; Cambridge University Press: Cambridge, UK, 2017; pp. 254–264. ISBN 978-1-107-14740-9.
28. Aubet, M.E. *The Phoenicians and the West: Politics, Colonies and Trade*, 2nd ed.; Cambridge University Press: Cambridge, UK, 2001.
29. Amadasi Guzzo, M.G. The Language. In *The Oxford Handbook of the Phoenician and Punic Mediterranean*; Doak, B.R., López-Ruiz, C., Eds.; Oxford University Press: Oxford, UK, 2019; ISBN 978-0-19-049934-1.
30. Xella, P. Religion. In *The Oxford Handbook of the Phoenician and Punic Mediterranean*; Doak, B.R., López-Ruiz, C., Eds.; Oxford University Press: Oxford, UK, 2019; ISBN 978-0-19-049934-1.
31. Bellard, C.G. Agriculture. In *The Oxford Handbook of the Phoenician and Punic Mediterranean*; Doak, B.R., López-Ruiz, C., Eds.; Oxford University Press: Oxford, UK, 2019; ISBN 978-0-19-049934-1.
32. Arruda, A.M. *Los Fenicios en Portugal. Fenicios e indígenas en el centro y sur de Portugal (siglos VIII-VI a.C.)*; Universidad Pompeu Fabra: Barcelona, Spain, 1999.
33. Arruda, A.M. O 1.º milénio a.n.e. no Centro e no Sul de Portugal: Leituras possíveis no início de um novo século. *Arqueólogo Port.* **2005**, *4*, 9–156.
34. Gomes, F. Mediterranean goods in “Post-Orientalizing” funerary contexts of Southern Portugal: Some remarks on consumption, peripherality and cultural identity. In *Actas del XVIII Congreso Internacional de Arqueología Clásica: Centro y Periferia en el Mundo Clásico*; Martínez, J.M.Á., Basarrate, T.N., Llanza, I.R., Eds.; National Museum of Roman Art: Mérida, Spain, 2015; Volume 1, pp. 435–438.
35. Costa, M.; Barrulas, P.; Arruda, A.M.; Dias, L.; Barbosa, R.; Vadenabeele, P.; Mirão, J. An Insight into the Provenance of the Phoenician-Punic Glass Beads of the Necropolis of Vinha Das Calijas (Beja, Portugal). *Archaeol. Anthropol. Sci.* **2021**, *13*, 17. [[CrossRef](#)]
36. García-Heras, M.; Rincón, J.M.; Jimeno, A.; Villegas, M.A. Pre-Roman Coloured Glass Beads from the Iberian Peninsula: A Chemico-Physical Characterisation Study. *J. Archaeol. Sci.* **2005**, *32*, 727–738. [[CrossRef](#)]
37. Gomes, F.B. Mediterranean Exotica and the Fabric of Early Iron Age Society in Western Iberia (8th–5th Centuries BCE). *Layers Archeol. Territ. Contesti* **2023**, *8*, 1–19. [[CrossRef](#)]
38. Dietler, M. Colonial Encounters in Iberia and the Western Mediterranean: An Exploratory Framework. In *Colonial Encounters in Ancient Iberia: Phoenician, Greek, and Indigenous Relations*; Dietler, M., López-Ruiz, C., Eds.; University of Chicago Press: Chicago, IL, USA, 2009; pp. 3–48.
39. Fletcher, R.N. Opening the Mediterranean: Assyria, the Levant and the Transformation of Early Iron Age Trade. *Antiquity* **2012**, *86*, 211–220. [[CrossRef](#)]
40. Wagner, C.G.; Alvar, J. La colonización agrícola en la península ibérica: Estado de la cuestión y nuevas perspectivas. In *Ecohistoria del Paisaje Agrario: La Agricultura Fenicio-Púnica en el Mediterráneo*; Bellard, C.G., Ed.; Universidad de Valencia/Universitat de València: Valencia, Spain, 2003; pp. 187–204. ISBN 978-84-370-5508-4.
41. Eshel, T.; Erel, Y.; Yahalom-Mack, N.; Tirosh, O.; Gilboa, A. Lead Isotopes in Silver Reveal Earliest Phoenician Quest for Metals in the West Mediterranean. *Proc. Natl. Acad. Sci. USA* **2019**, *116*, 6007–6012. [[CrossRef](#)] [[PubMed](#)]
42. Arruda, A.M. The Phoenicians in Portugal. In *The Oxford Handbook of the Phoenician and Punic Mediterranean*; López-Ruiz, C., Doak, B.R., Eds.; Oxford University Press: Oxford, UK, 2019.
43. Soares, A.M.M.; Arruda, A.M.; Barcleó, J.A.; Bogdanovic, I.; Morell, B. A cronologia de radiocarbono para a Idade do Ferro Orientalizante no território português. Uma leitura crítica dos dados arqueométricos e arqueológicos. In *IberCrono 2016 Cronometrías Para la Historia de la Península Ibérica (Chronometry for the History of the Iberian Peninsula)*; CEUR: Barcelona, Spain, 2017; Volume 2024, pp. 235–259.
44. López Castro, J.L. The Iberian Peninsula. In *The Oxford Handbook of the Phoenician and Punic Mediterranean*; Doak, B.R., López-Ruiz, C., Eds.; Oxford University Press: Oxford, UK, 2019; ISBN 978-0-19-049934-1.
45. Gomes, F.B. The West Writes Back: Cultural Contact and Identity Constructs in Southern Portuguese Late Bronze Age/Early Iron Age. In *The Mediterranean Mirror: Cultural Contacts in the Mediterranean Sea between 1200 and 750 B.C.*; Babbi, A., Bubbenheimer-Erhart, F., Marín-Aguilera, B., Mühl, S., Eds.; Römisch-Germanisches Zentralmuseum: Mainz, Germany, 2015; pp. 305–318.

46. Arruda, A.M. Necrópoles proto-históricas do sul de Portugal: O mundo oriental e orientalizante. O mundo funerario. In *Actas de III Seminario Internacional sobre Temas Fenicos, Alicante*; González Prats, A., Pellicer Catalán, M., Eds.; Generalitat Valenciana: Alicante, Spain, 2004; pp. 457–494.
47. Gomes, F.B.; Arruda, A.M. On the Edge of History? The Early Iron Age of Southern Portugal, between Texts and Archaeology. *World Archaeol.* **2019**, *50*, 764–780. [[CrossRef](#)]
48. Berrocal-Rangel, L.; Silva, C.A. *O Castro dos Ratinhos (Barragem de Alqueva, Moura): Excavações Num Povoado Proto-Histórico do Guadiano, 2004–2007*; O Archeólogo Português Suplemento; Museu Nacional de Arqueologia: Lisboa, Portugal, 2010; ISBN 978-972-9257-25-4.
49. Gomes, F.B. Cuentas de vidrio oculadas de la Edad del Hierro del sur de Portugal (ss. VII–II a. n. e.). *Trab. Prehist.* **2023**, *80*, e17. [[CrossRef](#)]
50. Arruda, A.; Barbosa, R.; Gomes, F.; Sousa, E. A Necrópole de Vinha das Calças (Beja, Portugal). In *Sidereum Ana III-El río Guadiana y Tartessos*; Ávila, J.J., Ed.; Consórcio de la Ciudad Monumental Histórico-Artística y Arqueológica de Mérida: Mérida, Mexico, 2016; pp. 187–225.
51. Gomes, F.B. O mundo funerário da Idade do Ferro no Sul do actual território português: Notas para uma síntese. *Arqueol. História* **2014**, *66–67*, 47–62.
52. Santos, F.J.; Antunes, A.S.; Deus, M.G. A necrópole de Palhais (Beringel, Beja). In *Sidereum Ana III-El río Guadiana y Tartessos*; Ávila, J.J., Ed.; Consórcio de la Ciudad Monumental Histórico-Artística y Arqueológica de Mérida: Mérida, Mexico, 2017; pp. 227–262.
53. Costa, M.; Arruda, A.M.; Dias, L.; Barbosa, R.; Mirão, J.; Vandenabeele, P. The Combined Use of Raman and Micro-X-Ray Diffraction Analysis in the Study of Archaeological Glass Beads. *J. Raman Spectrosc.* **2019**, *50*, 250–261. [[CrossRef](#)]
54. Biron, I.; Chopinet, M.H. Colouring, Decolouring, and Opacifying of Glass. In *Modern Methods for Analysing Archaeological and Historical Glass*; Janssens, K., Ed.; John Wiley & Sons, Ltd.: Chichester, UK, 2013; Volume 1, pp. 49–65.
55. Cosyns, P. *The Production, Distribution and Consumption of Black Glass in the Roman Empire during the 1st–5th Century AD: An Archaeological, Archaeometric and Historical Approach*, Faculteit Letteren en Wijsbegeerte; Vrije Universiteit Brussel: Brussel, Belgium, 2011.
56. Van Der Linden, V.; Cosyns, P.; Schalm, O.; Cagno, S.; Nys, K.; Janssens, K.; Nowak, A.; Wagner, B.; Bulska, E. Deeply Coloured and Black Glass in the Northern Provinces of the Roman Empire: Differences and Similarities in Chemical Composition Before and After AD150*. *Archaeometry* **2009**, *51*, 822–844. [[CrossRef](#)]
57. Cagno, S.; Cosyns, P.; Nys, K.; Janssens, K. Black-Appearing Roman Glass. In *Modern Methods for Analysing Archaeological and Historical Glass*; Janssens, K., Ed.; John Wiley & Sons, Ltd.: Chichester, UK, 2013; Volume 1, pp. 369–386.
58. Lankton, J.W.; Pulak, C.; Gratuze, B. Glass Ingots from the Uluburun Shipwreck: Glass by the Batch in the Late Bronze Age. *J. Archaeol. Sci. Rep.* **2022**, *42*, 103354. [[CrossRef](#)]
59. Nicholson, P.T.; Gerisch, R.; Brook, E.; Jackson, C.M. *Brilliant Things for Akhenaten: The Production of Glass, Vitreous Materials and Pottery at Amarna Site O45.1*; Excavation Memoir, Egypt Exploration Society: London, UK; David Brown Book Co.: Oakville, CT, USA, 2007; ISBN 978-0-85698-178-4.
60. Shortland, A.J.; Eremin, K. The Analysis of Second Millennium Glass from Egypt and Mesopotamia, Part 1: New Wds Analyses. *Archaeometry* **2006**, *48*, 581–603. [[CrossRef](#)]
61. Kemp, V.; Delbey, T.; Shortland, A. The Dating and Provenance of Glass Fragments from the Site of Serabit El-Khâdim, Sinai. *J. Archaeol. Sci. Rep.* **2023**, *49*, 103920. [[CrossRef](#)]
62. Franjić, A. *Iron Age Glass Technology in South East Europe*; UCL (University College London): London, UK, 2020.
63. Cagno, S.; Cosyns, P.; Der Linden, V.V.; Schalm, O.; Izmer, A.; Deconinck, I.; Vanhaecke, F.; Nowak, A.; Wagner, B.; Bulska, E.; et al. Composition Data of a Large Collection of Black-Appearing Roman Glass. *Open J. Archaeom.* **2013**, *1*, e22. [[CrossRef](#)]
64. Cagno, S.; Cosyns, P.; Izmer, A.; Vanhaecke, F.; Nys, K.; Janssens, K. Deeply Colored and Black-Appearing Roman Glass: A Continued Research. *J. Archaeol. Sci.* **2014**, *42*, 128–139. [[CrossRef](#)]
65. Pelicano, A. *Práticas Funerárias na Idade do Ferro. O Caso de Vinha das Calças 4, Trigaches*. Master’s Thesis, Universidade de Coimbra, Coimbra, Portugal, 2016.
66. Costa, M.; Arruda, A.M.; Barbosa, R.; Barrulas, P.; Vandenabeele, P.; Mirão, J. A Micro-Analytical Study of the Scarabs of the Necropolis of Vinha Das Calças (Portugal). *Microsc. Microanal.* **2019**, *25*, 214–220. [[CrossRef](#)] [[PubMed](#)]
67. Costa, M.; Barrulas, P.; Arruda, A.M.; Barbosa, R.; Vandenabeele, P.; Mirão, J. New Approaches for the Study of Faience Using Beads from Southern Portugal. *J. Archaeol. Sci. Rep.* **2022**, *46*, 103703. [[CrossRef](#)]
68. Ngan-Tillard, D.J.M.; Huisman, D.J.; Corbella, F.; Van Nass, A. Over the Rainbow? Micro-CT Scanning to Non-Destructively Study Roman and Early Medieval Glass Bead Manufacture. *J. Archaeol. Sci.* **2018**, *98*, 7–21. [[CrossRef](#)]
69. Medeghini, L.; Botticelli, M.; Cadena-Irizar, A.C.; Lepri, B.; Ferrandes, A.F.; Costa, M.; Barrulas, P. Blue Shadows of Roman Glass Artefacts. *Microchem. J.* **2022**, *179*, 107526. [[CrossRef](#)]
70. McGloin, J. Of Beads and Burials: A Microwear and Experimental Study of Early Medieval Glass and Amber Beads from the Merovingian Site of Lent-Lentseveld. *J. Archaeol. Sci.* **2021**. [[CrossRef](#)]
71. Purowski, T. Identifying Bronze Age Glass Production Centres through Bead-Making Techniques. *Archeol. Pol.* **2022**, *67*, 61–80. [[CrossRef](#)]

72. Venclová, N. *Prehistoric Glass in Bohemia*; Archeologický ústav ČSAV: Praha, Czech Republic, 1990.
73. Yatsuk, O.; Gorghinian, A.; Fiocco, G.; Davit, P.; Francone, S.; Serges, A.; Koch, L.; Re, A.; Lo Giudice, A.; Ferretti, M.; et al. Ring-Eye Blue Beads in Iron Age Central Italy—Preliminary Discussion of Technology and Possible Trade Connections. *J. Archaeol. Sci. Rep.* **2023**, *47*, 103763. [[CrossRef](#)]
74. Koch, L.C. Zur Herstellungstechnik Der Perlen. In *Früheisenzeitliches Glas und Glasfunde Mittelitaliens: Eine Übersicht von der Villanovazeit bis zum Orientalizzante und eine Analyse der Glasperlen als Grabbeigabe des Gräberfeldes Quattro Fontanili in Veji*; Bochumer Forschungen zur ur- und frühgeschichtlichen Archäologie; Verlag Marie Leidorf: Rahden, Germany, 2011; pp. 28–31.
75. Cox, G.A.; Ford, B.A. The Long-Term Corrosion of Glass by Ground-Water. *J. Mater. Sci.* **1993**, *28*, 5637–5647. [[CrossRef](#)]
76. Fernández-Navarro, J.-M.; Villegas, M.-Á. *What Is Glass?* Janssens, K., Ed.; John Wiley & Sons, Ltd.: Chichester, UK, 2013; Volume 1.
77. Melcher, M.; Schreiner, M. Glass Degradation by Liquids and Atmospheric Agents. In *Modern Methods for Analysing Archaeological and Historical Glass*; Janssens, K., Ed.; John Wiley & Sons, Ltd.: Chichester, UK, 2013; Volume 1, pp. 609–652.
78. Gratuze, B.; Janssens, K. Provenance Analysis of Glass Artefacts. In *Comprehensive Analytical Chemistry*; Janssens, K., Grieken, R., Eds.; Elsevier Science: Amsterdam, The Netherlands, 2004; Volume 42, pp. 663–712.
79. Stern, W.B. Phosphate: A Neglected Argument in Studies of Ancient Glass Technology. *Swiss J. Geosci.* **2017**, *110*, 725–740. [[CrossRef](#)]
80. Eremin, K.; Degryse, P.; Erb-Satullo, N.; Ganio, M.; Greene, J.; Shortland, A.; Walton, M.; Stager, L. Iron Age Glass Beads from Carthage. In *Historical Technology, Materials, and Conservation: SEM and Microanalysis*; Meeks, N.D., Meek, A., Eds.; Archetype Publications and the British Museum: London, UK, 2012; pp. 30–35.
81. Brems, D.; Degryse, P. Trace Element Analysis in Provenancing Roman Glass-Making. *Archaeometry* **2014**, *56*, 116–136. [[CrossRef](#)]
82. Agua, F.; Conde, J.F.; Kobylińska, U.; Kobyliński, Z.; García-Heras, M.; Villegas, M.-Á. Chemical-Physical Characterisation of Early Iron Age Glass Beads from Central Europe. *Bol. Soc. Esp. Cerámica Vidr.* **2017**, *56*, 119–130. [[CrossRef](#)]
83. Braun, C. Analyse von Gläsern Aus Der Hallstattzeit Mit Einem Excurs Über Römische Fenstergläser. In *Glasperlen der vorrömischen Eisenzeit Vol. 1. Marburger Studien zur Vor- und Frühgeschichte 5*; Haevernick, T.E., Frey, O.-H., Eds.; Verlag Phillip von Zabern: Mainz am Rhein, Germany, 1983; pp. 129–175.
84. Conte, S.; Matarese, I.; Vezzalini, G.; Pacciarelli, M.; Scarano, T.; Vanzetti, A.; Gratuze, B.; Arletti, R. How Much Is Known about Glassy Materials in Bronze and Iron Age Italy? New Data and General Overview. *Archaeol. Anthropol. Sci.* **2019**, *11*, 1813–1841. [[CrossRef](#)]
85. Degryse, P.; Shortland, A.J. Interpreting Elements and Isotopes in Glass: A Review. *Archaeometry* **2020**, *62*, 117–133. [[CrossRef](#)]
86. Foy, D.; Picon, M.; Vichy, M. Verres Omeyyades et Abbasides d'origine Egyptienne: Les temoignages de l'archéologie et de l'archéométrie. In *Annales du 15e Congrès de l'Association Internationale pour l'Histoire du Verre*; AIHV: Nottingham, UK, 2003; Volume 15, pp. 138–143.
87. Brems, D.; Degryse, P.; Hasendoncks, F.; Gimeno, D.; Silvestri, A.; Vassilieva, E.; Luypaers, S.; Honings, J. Western Mediterranean Sand Deposits as Raw Material for Roman Glass Production. *J. Archaeol. Sci.* **2012**, *39*, 2897–2907. [[CrossRef](#)]
88. Brems, D.; Degryse, P. Western Mediterranean Sands for Ancient Glass Making. In *Glass Making in the Greco-Roman World: Results of the ARCHGLASS Project*; Degryse, P., Ed.; Leuven university Press: Leuven, Belgium, 2015; pp. 27–50.
89. Turner, W.E.S. Studies in Ancient Glasses and Glass Making Processes. Part V. Raw Materials and the Melting Process. *J. Soc. Glass Technol.* **1956**, *40*, 277–300.
90. Cormier, L. Glasses: Aluminosilicates. In *Encyclopedia of Materials: Technical Ceramics and Glasses*; Pomeroy, M., Ed.; Elsevier: Oxford, UK, 2021; pp. 496–518. ISBN 978-0-12-822233-1.
91. Freestone, I.C.; Leslie, K.A.; Thirlwall, M.; Gorin-Rosen, Y. Strontium Isotopes in the Investigation of Early Glass Production: Byzantine and Early Islamic Glass from the Near East*. *Archaeometry* **2003**, *45*, 19–32. [[CrossRef](#)]
92. Martignier, A.; Filella, M.; Pollok, K.; Melkonian, M.; Bensimon, M.; Barja, F.; Langenhorst, F.; Jaquet, J.-M.; Ariztegui, D. Marine and Freshwater Micropearls: Biomineralization Producing Strontium-Rich Amorphous Calcium Carbonate Inclusions Is Widespread in the Genus *Tetraselmis* (Chlorophyta). *Biogeosciences* **2018**, *15*, 6591–6605. [[CrossRef](#)]
93. Otter, L.M.; Agbaje, O.B.A.; Kilburn, M.R.; Lenz, C.; Henry, H.; Trimby, P.; Hoppe, P.; Jacob, D.E. Insights into Architecture, Growth Dynamics, and Biomineralization from Pulsed Sr-Labelled *Katylsia Rhytiphora* Shells (Mollusca, Bivalvia). *Biogeosciences* **2019**, *16*, 3439–3455. [[CrossRef](#)]
94. Wedepohl, K.H. The Chemical Composition Including the Rare Earth Elements of the Three Major Glass Types of Europe and the Orient Used in Late Antiquity and the Middle Ages. *Chem. Erde* **2011**, *71*, 289–296. [[CrossRef](#)]
95. Silvestri, A.; Molin, G.; Salviulo, G. The Colourless Glass of Iulia Felix. *J. Archaeol. Sci.* **2008**, *35*, 331–341. [[CrossRef](#)]
96. Foster, H.E.; Jackson, C.M. The Composition of Late Romano-British Colourless Vessel Glass: Glass Production and Consumption. *J. Archaeol. Sci.* **2010**, *37*, 3068–3080. [[CrossRef](#)]
97. Freestone, I.C. The Recycling and Reuse of Roman Glass: Analytical Approaches. *J. Glass Stud.* **2015**, *57*, 29–40.
98. Freestone, I.C.; Ponting, M.; Hughes, M.J. The Origins of Byzantine Glass from Maroni Petrera, Cyprus. *Archaeometry* **2002**, *44*, 257–272. [[CrossRef](#)]

99. Gliozzo, E. The Composition of Colourless Glass: A Review. *Archaeol. Anthropol. Sci.* **2017**, *9*, 455–483. [[CrossRef](#)]
100. Bliem, R.; Pavelec, J.; Gamba, O.; McDermott, E.; Wang, Z.; Gerhold, S.; Wagner, M.; Osiecki, J.; Schulte, K.; Schmid, M.; et al. Adsorption and Incorporation of Transition Metals at the Magnetite Fe₃O₄ (001) Surface. *Phys. Rev. B* **2015**, *92*, 075440. [[CrossRef](#)]
101. Zhong, Y.; Liang, X.; Tan, W.; Zhong, Y.; He, H.; Zhu, J.; Yuan, P.; Jiang, Z. A Comparative Study about the Effects of Isomorphous Substitution of Transition Metals (Ti, Cr, Mn, Co and Ni) on the UV/Fenton Catalytic Activity of Magnetite. *J. Mol. Catal. Chem.* **2013**, *372*, 29–34. [[CrossRef](#)]
102. Giannini, R.; Freestone, I.C.; Shortland, A.J. European Cobalt Sources Identified in the Production of Chinese Famille Rose Porcelain. *J. Archaeol. Sci.* **2017**, *80*, 27–36. [[CrossRef](#)]
103. Gratuze, B.; Pactat, I.; Schibille, N. Changes in the Signature of Cobalt Colorants in Late Antique and Early Islamic Glass Production. *Minerals* **2018**, *8*, 225. [[CrossRef](#)]
104. Rodríguez González, E.; Celestino Pérez, S.; Medina Sánchez, M.C.; Zucchiatti, A.; Barrio Martín, J. Trade with the West. Glass Bowls of Eastern Mediterranean Origin Found in the Courtyard of the Casas Del Turuñuelo Site (Guareña, Badajoz, Spain): Archaeological Context, Analysis and Conservation. *J. Archaeol. Sci. Rep.* **2023**, *50*, 104029. [[CrossRef](#)]
105. Oikonomou, A.; Triantafyllidis, P. An Archaeometric Study of Archaic Glass from Rhodes, Greece: Technological and Provenance Issues. *J. Archaeol. Sci. Rep.* **2018**, *22*, 493–505. [[CrossRef](#)]
106. Franjic, A.; Freestone, I.; Križ, B.; Stipančić, P. The Spectrometric Analysis of Iron Age Glass Beads from Novo Mesto, Slovenia | Spektrometrične Analize Železnodobnih Steklenih Jagod Iz Novega Mesta, Slovenija. *Stud. Univ. Hered. Znan. Rev. Za Raziskave Teor. Kult. Dediščine* **2022**, *10*, 23–29. [[CrossRef](#)]
107. Schibille, N.; De Juan Ares, J.; Casal García, M.T.; Guerrot, C. Ex Novo Development of Lead Glassmaking in Early Umayyad Spain. *Proc. Natl. Acad. Sci. USA* **2020**, *117*, 16243–16249. [[CrossRef](#)]
108. Miazga, B.; Duma, P.; Cembrzyński, P.; Matyszczyk, M.; Piekalski, J. Analytical Studies on Medieval Lead Ingots from Wrocław and Kraków (Poland): A Step towards Understanding Bulk Trade of Lead from Kraków and Silesia Upland Pb–Zn Deposits. *Herit. Sci.* **2022**, *10*, 184. [[CrossRef](#)]
109. Wedepohl, K.H.; Baumann, A. Isotope Composition of Medieval Lead Glasses Reflecting Early Silver Production in Central Europe. *Miner. Deposita* **1997**, *32*, 292–295. [[CrossRef](#)]
110. Pactat, I.; Guérit, M.; Simon, L.; Gratuze, B.; Raux, S.; Aunay, C. Evolution of Glass Recipes during the Early Middle Ages in France: Analytical Evidence of Multiple Solutions Adapted to Local Contexts. In *Annales du 20e congrès de l'Association Internationale Pour l'Histoire du Verre: Fribourg/Romont, 7–11 Septembre 2015*; Wolf, S., De Pury-Gysel, A., Eds.; Verlag Marie Leidorf GmbH: Rahden, Germany, 2017; pp. 334–340.
111. Anguilano, L.; Rehren, T.; Müller, W.; Rothenberg, B. The Importance of Lead in the Silver Production at Riotinto (Spain). *ArcheoSciences Rev. Archéom.* **2010**, *34*, 269–276. [[CrossRef](#)]
112. Kaufman, B.; Docter, R.; Fischer, C.; Chelbi, F.; Maraoui Telmini, B. Ferrous Metallurgy from the Bir Massouda Metallurgical Precinct at Phoenician and Punic Carthage and the Beginning of the North African Iron Age. *J. Archaeol. Sci.* **2016**, *71*, 33–50. [[CrossRef](#)]
113. Lahlil, S.; Biron, I.; Cotte, M.; Susini, J.; Menguy, N. Synthesis of Calcium Antimonate Nano-Crystals by the 18th Dynasty Egyptian Glassmakers. *Appl. Phys. Mater. Sci. Process.* **2010**, *98*, 1–8. [[CrossRef](#)]
114. Lahlil, S.; Biron, I.; Galoisy, L.; Morin, G. Rediscovering Ancient Glass Technologies through the Examination of Opacifier Crystals. *Appl. Phys. Mater. Sci. Process.* **2008**, *92*, 109–116. [[CrossRef](#)]
115. Vandini, M.; Fiorentino, S. From Crystals to Color: A Compendium of Multi-Analytical Data on Mineralogical Phases in Opaque Colored Mosaic Tesserae. *Minerals* **2020**, *10*, 609. [[CrossRef](#)]
116. Shortland, J. The Use and Origin of Antimonate Colorants in Early Egyptian Glass. *Archaeometry* **2002**, *44*, 517–530. [[CrossRef](#)]
117. Lahlil, S.; Biron, I.; Cotte, M.; Susini, J. New Insight on the in Situ Crystallization of Calcium Antimonate Opacified Glass during the Roman Period. *Appl. Phys. Mater. Sci. Process.* **2010**, *100*, 683–692. [[CrossRef](#)]
118. Truffa Giachet, M.; Gratuze, B.; Ozainne, S.; Mayor, A.; Huysecom, E. A Phoenician Glass Eye Bead from 7th–5th c. Cal BCE Nin-Bère 3, Mali: Compositional Characterisation by LA-ICP-MS. *J. Archaeol. Sci. Rep.* **2019**, *24*, 748–758. [[CrossRef](#)]
119. Shortland, A.; Rogers, N.; Eremin, K. Trace Element Discriminants between Egyptian and Mesopotamian Late Bronze Age Glasses. *J. Archaeol. Sci.* **2007**, *34*, 781–789. [[CrossRef](#)]
120. Freestone, I.; Gorin-Rosen, Y.; Hughes, M.J. Primary glass from Israel and the Production of Glass in Late Antiquity and the Early Islamic Period, La Route du verre. Ateliers primaires et secondaires du second millénaire av. J.-C. au Moyen Âge. Colloque organisé en 1989 par l'Association française pour l'Archéologie du Verre (AFAV). *Lyon Maison Orient Méditerranée Jean Pouilloux* **2000**, *33*, 65–83.
121. Schibille, N.; Gratuze, B.; Ollivier, E.; Blondeau, É. Chronology of Early Islamic Glass Compositions from Egypt. *J. Archaeol. Sci.* **2019**, *104*, 10–18. [[CrossRef](#)]
122. Wedepohl, K.H. The Composition of the Continental Crust. *Cosmochim. Acta* **1995**, *59*, 1217–1232. [[CrossRef](#)]
123. Blomme, A.; Elsen, J.; Brems, D.; Shortland, A.; Dotsika, E.; Degryse, P. Tracing the Primary Production Location of Core-Formed Glass Vessels, Mediterranean Group I. *J. Archaeol. Sci. Rep.* **2016**, *5*, 1–9. [[CrossRef](#)]

124. D’Oriano, C.; Da Pelo, S.; Podda, F.; Cioni, R. Laser-Ablation Inductively Coupled Plasma Mass Spectrometry (LA-ICP-MS): Setting Operating Conditions and Instrumental Performance. *Period. Mineral.* **2008**, *77*, 65–74. [[CrossRef](#)]
125. Pearce, N.J.; Perkins, W.T.; Westgate, J.A.; Gorton, M.P.; Jackson, S.E.; Neal, C.R.; Chenery, S.P. A Compilation of New and Published Major and Trace Element Data for NIST SRM 610 and NIST SRM 612 Glass Reference Materials. *Geostand. Newsl.* **1997**, *21*, 115–144. [[CrossRef](#)]

Disclaimer/Publisher’s Note: The statements, opinions and data contained in all publications are solely those of the individual author(s) and contributor(s) and not of MDPI and/or the editor(s). MDPI and/or the editor(s) disclaim responsibility for any injury to people or property resulting from any ideas, methods, instructions or products referred to in the content.